sustainability

MDPI

Article

Synthesis, Stability and Microstructure of a One-Step Mixed Geopolymer Backfill Paste Derived from Diverse Waste Slags

Xianhui Zhao [1], Haoyu Wang [2,*], Han Gao [3], Luhui Liang [1] and Jing Yang [1]

[1] School of Civil Engineering, Hebei University of Engineering, Handan 056038, China; zhaoxianhui@hebeu.edu.cn (X.Z.)
[2] School of Civil Engineering, Tianjin Renai College, Tianjin 301636, China
[3] School of Mechanical Engineering, Tianjin Renai College, Tianjin 301636, China
* Correspondence: wanghaoyu@tjrac.edu.cn

Abstract: The advent of industrialization has produced an enormous amount of industrial waste slag, which drastically pollutes environmental resources. This study examines the production, stability, and microstructure of a novel backfill geopolymer paste derived from multiple industrial waste slags, including silica-alumina precursors (low-calcium composition) and waste slags (high-calcium composition), as well as two additives. The characteristics of self-hardening were discovered. The effects of low-calcium fly ash, granulated blast furnace slag, red mud, and lime powder on fluidity and compressive strength were then evaluated. To assess the stability, the resistances to drying shrinkage, permeability, and chemical attack by an optimized geopolymer backfill paste were investigated. Furthermore, SEM-EDS, XRD, FTIR, and TG-DSC tests were employed to reveal the microstructures, products, and thermal stability. The results show that the backfill paste hardens well and has no impact on alkalinity dissolution for adjacent soils and water. The optimum sample, P1, had a water-binder ratio of 0.70, resulting in 201 mm fluidity and 2.1 MPa 28-d compressive strength. In terms of drying shrinkage, permeability, and Na_2SO_4 and NaCl solution attack, sample P1 outperformed the conventional Ordinary Portland cement paste (OPC) for 90 days. The paste P1 containing about 46.0 wt% waste slags meets the fresh and hardened property requirements for goaf backfill, and the chemical binding of P1 is acquired from the mixture of (N,C)-A-S-H, C-S-H, and C-A-S-H gel products. These findings lay the groundwork for the scientific application of a wide range of waste slags in backfill engineering.

Keywords: backfill materials; waste slags; geopolymer; mixing proportion; stability; compressive strength; microstructures

check for updates

Citation: Zhao, X.; Wang, H.; Gao, H.; Liang, L.; Yang, J. Synthesis, Stability and Microstructure of a One-Step Mixed Geopolymer Backfill Paste Derived from Diverse Waste Slags. *Sustainability* **2023**, *15*, 6708. https://doi.org/10.3390/su15086708

Academic Editor: Silvia Fiore

Received: 18 February 2023
Revised: 11 March 2023
Accepted: 14 April 2023
Published: 15 April 2023

Copyright: © 2023 by the authors. Licensee MDPI, Basel, Switzerland. This article is an open access article distributed under the terms and conditions of the Creative Commons Attribution (CC BY) license (https://creativecommons.org/licenses/by/4.0/).

1. Introduction

The manufacturing material Ordinary Portland Cement (OPC) is the most commonly used cementitious product in the building sector. However, the OPC manufacturing process produces significant amounts of CO_2 gas, posing an environmental risk [1,2]. Approximately 950 kg of CO_2 are emitted for each one thousand kilograms of OPC synthesized [3]. In North China, increasingly stringent government restrictions limit the production and use of Portland cement [4,5]. In addition, the treatment of solid wastes, such as fly ash (FA) in power plants and other slags in manufacturing-businesses, constitutes a significant environmental and social problem. The bulk of industrial solid wastes is still left in the open, endangering the local air, water, and land ecosystems, even though a lot of FA and slag have been recycled into cement, concrete, and geotechnical materials [6–9]. For industrial wastes such as FA and slag, amongst others, to be utilized as a replacement for Portland cement to the greatest extent feasible, research and development of novel cementitious materials are required to find solutions to the challenges described above.

In order to create geopolymers, FA, also known as granulated blast furnace slag (GBFS), and several other silica-alumina precursors are subjected to alkali activation [10,11].

Due to their better mechanical performance, low energy requirements, and negligible impact on the environment, geopolymers are being evaluated as sustainable substitutes for Portland cement [12–16]. Geopolymers have the potential to cut down carbon dioxide emissions and energy use by up to 80% and 60%, respectively [17,18]. Using geopolymer materials made from industrial waste instead of Portland cement in Australia has reduced costs by 7% (not including transporting costs) while reducing carbon dioxide emissions by 44% [19,20]. As a result of the 25 yuan per ton charge placed on businesses for incorrect treatment and disposal, the disposal of industrial wastes from coal combustion and steel operations, among others, has become more common since the introduction and enforcement of the Environmental Protection Charge Law (China) in 2018 [9]. Recent years have seen the intensive study of geopolymer materials derived from discarded industrial solid waste [21–23].

Common two-part geopolymers were synthesized by using the mixtures of strong alkaline solution (M) and silica-alumina solid precursors (Si-O and Al-O) [24,25], by the empirical expression $M_x[-(SiO_2)_y-(AlO_2)-]_x$ [6] for geopolymer gels. Nevertheless, it is important to note that while making and using two-part geopolymers, the high corrosion rate of alkaline solutions as activators have to be taken into account, and strict protective measures need to be taken. The restriction on the use of alkaline solutions is very detrimental to the massive synthesis and use of geopolymer materials that are derived from industrial waste. In the past few years, a one-part geopolymer has gained popularity as a material that is both risk-free and simple to work with. This material may be produced by combining solid binders with water [11,25,26]. Conventional Portland cement slurry is produced identically to one-part geopolymer paste [11]. Certain particles in a one-part geopolymer undergo alkali-activation as soon as water is introduced to the mixture. This causes the silica-alumina components to become more reactive. In order to manufacture one-part geopolymer binders, the silica-alumina components (which may include things like FA, red mud, slag, and so on) and the solid activators were mixed together in a consistent manner before being brought to use. In the past few years, a considerable amount of research has been carried out in an effort to reduce the expense of strong alkaline activation and make headway in resolving the issue that it presents. This has been accomplished by using a variety of alkaline solid wastes as replacements for Portland cement in the production of innovative binders [10].

In addition, China is home to a wide array of industrial solid wastes, including low-calcium silica-alumina byproducts and high-calcium waste slags, amongst others. Fly ash (FA) and red mud (RM) are both examples of frequent reactive byproducts that include low calcium levels and high levels of silica and alumina. Around 500 million tons of FA are commercially available in China each year from a variety of enterprises [27,28]. The estimated 2.7 billion tons of RM leftovers in the world's reserves are still growing each year at a rate of 120 million tons [18,29]. In addition, waste slags like soda residue (SR), carbide slag (CSG), and granulated blast furnace slag (GBFS) have between 40% and 90% CaO. The SRs are manufactured via the Na_2CO_3 industrial method, and around 7.8 to 10.0 million tons of SRs are discharged annually by over 50 Chinese companies [8,9]. For every ton of PVC produced, around 1.5 to 1.9 tons of CSG are produced. In addition, China's current CSG reserve surpasses 10 million tons [30]. As a result, the development and implementation of novel techniques of storage and remediation, and the pursuit of large-volume usage options for RM, FA, CSG, and SR as hazardous industrial byproducts, are becoming increasingly important from an environmental protection and local strategy perspective.

In addition, research has been done to determine whether or not it would be possible to use such solid waste-based paste as backfill materials by using an alkali-activated technique [31]. High-calcium SR and CSG were used in the formulation of the FA-based geopolymer paste in order to enhance the fresh and hardened performances of the paste. Grouting backfill paste was created by combining SR and FA in experimental programs; the optimal paste, designated SFN6, had desirable properties such as a high stone ratio

(98.6%), high fluidity (260 mm), and high compressive strength (3.70 MPa) [9]. Moreover, CSG was used to enhance the physical, mechanical, and microstructural characteristics of FA-based geopolymers [7] by long-term curing. Due to their comparable chemical components, the reuse of CSG as an alternative to hydrated lime was investigated for the activation of GBFS [2]. System reactivity may be enhanced by combining calcium-rich alumina-silicates like GBFS with low-reactive precursors like low-calcium FA [28,32]. Although GBFS does serve as a partial replacement for FA, the increased concentration of reactive CaO is the most notable difference. This component is known to be beneficial in enhancing mechanical behavior in alkali-activated materials [33,34]. Additionally, RM is regarded to be appropriate for the synthesis of geopolymers due to its high alkaline content and high quality aluminates. To produce the geopolymer, RM and FA were combined with a composite activator and stirred [18,26,35]. The $Ca(OH)_2$ and CaO are potential substitutes to alkaline activators that may be used as admixtures or activators. This is due to the fact that the ingredients of $Ca(OH)_2$ and CaO are much less costly than NaOH and Na_2SiO_3 [36,37]. Because of the following challenges, it is currently not possible to bring the alkali-activated binder to the market in its commercial form: (1) the finding of new chemical admixtures; (2) the guarantee of workability, durability, and a proven track record in service; and (3) the lack of in depth information about the chemical properties of the materials [12]. According to the aforementioned investigations, there is still a dearth of understanding about the preparation process and assessment of the stability of cementitious materials made from more than four solid wastes.

Consequently, the primary objective of this research was to utilize diverse industrial solid wastes as geopolymer backfill pastes for goafs. Geopolymer backfill pastes were produced by combining various solid wastes (CSG, SR, FA, RM, etc.) with water. To examine the impacts of the self-hardening of paste and the functions of raw binders, the fluidity, electrical conductivity, setting time, and compressive strength of fresh and hardened paste properties were explored. In addition, the stability of drying shrinkage, permeability, and chemical attack by Na_2SO_4 and NaCl solutions were tested and compared to those of OPC paste. Furthermore, SEM-EDS, XRD, FTIR, and TG-DSC tests were used to examine the microstructure, product, stability, and cementation mechanism. This provided some instances of various solid wastes that may be utilized as backfill materials in engineering projects.

2. Experimental

2.1. Raw Materials

Raw materials including low-calcium silica-alumina precursors and high-calcium-based slags, in addition to two additives, are used in the manufacturing process of geopolymer backfill pastes. The used low-calcium silica-alumina precursors in this study are class I fly ash (labeled FFAI), class II fly ash (labeled FFAII), as well as red mud (labeled RM). The high-calcium slags that are used include carbide slag, also known as CSG, soda residue, also known as SR, granulated blast furnace slag, also known as GBFS, as well as briquette residue slag (labeled BRS). In addition to this, lime powder and gypsum powder (both abbreviated as LP and GP, respectively) are used. The term "diverse solid wastes" refers to the many solid combinations of FFAI, FFAII, RM, CSG, SR, and BRS that are produced from a wide range of industrial outputs. The X-ray fluorescence technique was employed to determine the chemical components of these materials (Table 1), and Table 2 lists the physical properties.

Table 1. The chemical compositions of raw materials measured by XRF (mass%). LOI is loss on ignition at 1000 °C.

Materials	SiO_2	Al_2O_3	CaO	Fe_2O_3	MgO	K_2O	SO_3	Na_2O	P_2O_5	TiO_2	Cl^-	Other	LOI
FFAI	53.6	33.5	2.8	0	1.6	1.5	0.9	0	0.4	1.3	0	1.5	3
FFAII	46.1	23.2	5.4	8	2.6	1.8	0.8	0	0.6	0.3	0	3.5	7.6
RM	27.5	28.4	2.5	25.8	0.2	0.1	0.8	14.7	0	0	0	0	0
CSG	8.7	0.5	62.6	1	1.7	0	0	0	0	0	0	0	25.4
BRS	14.7	1.2	72.6	1.1	0	0	1.4	0	0	0	0	4.7	4.3
SR	9.2	8.7	36.4	3.4	6.8	0.3	5.5	3.9	0	0.1	23.1	0	2.8
GBFS	35.1	16.2	33.6	0	11.1	0	0	0	0	0	0	4.1	0
GP	3	3.6	30.5	0	0.3	0	40.6	0.3	0	0	2.3	0	19.5
LP	0.1	0	71.2	0	1.8	0	1.6	0	0	0	0	0	25.3
OPC	21.8	5.7	65.3	3.5	0	0	2.8	0	0	0	0	0	0.9

Note: FFAI is class I fly ash. FFAII is class II fly ash. RM is red mud. CSG is carbide slag. BRS is briquette residue slag. SR is soda residue. GBFS is granulated blast furnace slag. GP is gypsum powder, LP is lime powder, and OPC is ordinary Portland cement (#325).

Table 2. The physical properties of raw materials.

Materials	pH (−)	EC (μS/cm)	SSA (m^2/kg)	SG (−)
FFAI	10.24	1075.0	640	2.48
FFAII	8.30	2750.0	390	2.25
RM	10.52	2180.0	360	2.56
CSG	8.55	2700.0	420	1.80
BRS	10.07	1632.0	345	1.10
SR	9.32	3710.0	307	2.35
GBFS	11.45	440.0	660	2.67
GP	8.25	4.6	300	2.98
LP	12.86	7580.0	320	1.10
OPC	12.87	8970.0	370	2.89

Note: Both the pH and the EC were determined at the same mass ratio of 1:5 for the solids to water. pH represents the mean pH (−), EC denotes the mean EC (S/cm), SSA represents the specific surface area (m^2/kg), and SG is now the specific gravity (−).

(1) Low-calcium silica-alumina precursors

A Chinese power plant at Gongyi, which is located in the province of Henan, was the source of Class I fly ash (FFAI). Considering that FFAI contains 2.8% CaO, it was regarded to be class F fly ash. The maximum size of the particles was 10.0 μm, while the average size of the particles was 2.0 μm. In accordance with the Chinese standard GB/T 1596-2017, the sieved residual from 45.0 μm should be less than 12%, and the limit of allowable LOI for FFAI should be less than 5%. A power station in Handan, which is located in the Hebei Province of China, was the source of Class II Fly ash (FFAII). The FFAII that has 5.4% CaO is likewise considered to be class F fly ash according to its composition. In addition, the fly ash had an average particle size of 15.0 μm, which designates it as class II fly ash in terms of fineness (i.e., the sieved residual from 45.0 μm was less than 30% and the LOI was less than 8%, in accordance with the GB/T 1596-2017). Both FFAII and FFAI had identical chemical compositions, with the exception of the presence of Fe_2O_3, although the FFAII had a much higher fineness and LOI than the FFAI. Red mud (RM) was provided by an aluminum production company in Gongyi, Henan Province, China. The RM and FA were activated by an alkaline solution to generate the geopolymer material [26,35] due to their comparable chemical compositions and potential reactivity. The RM includes SiO_2, Al_2O_3, and Fe_2O_3, and it had greater alkalinity (Na_2O).

(2) High-calcium-based slags

The production of the backfill paste requires the use of four distinct types of high-calcium-based slags, namely CSG, SR, GBFS, and BRS. The chosen CSG was obtained using a production process that is concentrated in the PVC manufacturing sector [7], and it was

supplied by a chemical industrial plant located in Qinghai, China, that manufactures C_2H_2. The CaO content, 62.6%, of the CSG results in its classification as a category II industrial solid waste. In addition, the SR came from a factory that makes Na_2CO_3 and is located in Tangshan, which is in the province of Hebei in China [8]. The SR has been found to include as much as 36.4% CaO along with a number of soluble salts including Cl^- and $SO_4{}^{2-}$. The GBFS of grade S95 is also supported in the city of Gongyi, which is located in the province of Henan in China. The GBFS was made up of 35.1% silicon dioxide, 16.2% aluminum oxide, and 33.6% calcium oxide. The fineness of 800 mesh was employed, and the grade that was used was S95 GBFS. The GBFS is a byproduct of industry, however it has a high reactivity to enhance hydration [10], despite the fact that it is a byproduct. The BRS is the slag that is left over after a civil briquette has been burned at temperatures between 800 and 1400 degrees Celsius [38,39]. The civil briquette is used to encourage the development of cleaner energy as an alternative to traditional coal. In terms of the chemical components that compose it, BRS has the same potential for reactivity as CSG. The BRS receives its coal from a factory located in Handan, which is located in the province of Hebei in China. The BRS was made up of SiO_2 (14.7%), Al_2O_3 (1.2%), and CaO (72.6%) as its three primary components.

(3) Additives for backfill paste

The GP and LP were provided by China's Xueli Building Material Enterprise in Tianjin. Without any processing, the GP (purity $\geq$ 71.1%) and LP (purity $\geq$ 71.2%) were introduced to the backfill paste as two additives. The GP (expressed as $CaSO_4{\cdot}2H_2O$) has minor expansion characteristics [40], including 30.5% CaO and 40.6% SO_3 by mass. The LP has excellent water absorption and hydration reactivity because of its high CaO content (71.2% by mass). As $Ca(OH)_2$ is the hydrated form of CaO, it is proposed that CaO may be a substantially more effective activator than $Ca(OH)_2$ based on the large difference in the strength of alkali-activated GBFS samples [12].

(4) Cement material comparison

Ordinary Portland cement (OPC) #325 was used as a comparison group for the backfill paste. The OPC, composed of 65.3% CaO and 21.8% SiO_2, was supplied by a building material company in Handan, Hebei Province, China.

(5) Sodium hydroxide pellet and water

In the tests being compared, the sodium hydroxide (NaOH) pellets utilized were white particle reagents (analytical grade, purity $\geq$ 98%) that are regarded as alkaline activators. China's Kemiou Company in Tianjin provided the NaOH pellets. In addition, in Handan city, Hebei Province, China, tap water with a pH of 7.40 and an electrical conductivity of 80.00 S/cm was used.

2.2. Mixing Design and Sample Preparation

2.2.1. Sample Preparation Method

The low-calcium silica-alumina precursors (FFAI, FFAII, and RM), high-calcium-based slags (CSG, SR, GBFS, and BRS), additives (GP and LP), and tap water were used in the formulation of the backfill grouting pastes. The chosen method of preparation is simple and functional from beginning to finish, beginning with the mixing of raw materials, and concluding with the demolding of samples once they have become firm. After combining all the solid raw ingredients in the proportions that were indicated for mixing, the required amount of tap water was added according to the water-to-binder ratio (W/B) that was designed. This allowed for the generation of a mixture that was consistent throughout. In order to generate a new paste, a one-step mixing technique was used to combine the materials, and the resulting mixture was then mixed at room temperature for three minutes. According to the prior research [9], the one-step mixing technique refers to the procedure of adding water to a solid mixture only once. This is analogous to the approach that is used in the preparation of a one-part geopolymer [11,26]. After being stirred, the freshly

formed pastes were poured into molds of varying sizes and placed in an environment with a temperature of 20 ± 2 degrees Celsius and a humidity of 100 percent. After being allowed to cure for the prescribed time, the dried and hardened paste samples were removed from their molds. Herein, the mixing time of three minutes is an important parameter for our experimental design. In the test, it was found that 3 min of mixing was sufficient to make the backfill net slurry well mixed, and if the time was too long, it affected the fluidity.

2.2.2. Mixing Ratio Design

(1) Twelve samples for self-hardening

In this research, twelve sets of pastes with arbitrary mixing proportions were created to test the self-hardening feasibility of pastes generated from different solid wastes by adding water, which also helps to identify the approximate mixing scope of each material. The backfill pastes were created utilizing a one-step mixing procedure under identical curing conditions (20 ± 2 °C in temperature and 100% humidity). The same 200 g of water was used to obtain good fluidity. Randomly recommended backfill paste mixing proportions are shown in Table 3. Fresh pastes were poured into steel molds with dimensions of 30 mm × 30 mm × 30 mm to create cubes. On this occasion, the OPC paste was likewise produced using 1250 g cement, 750 g water, and a water-to-cement ratio of 0.6. Due to the difference in water absorption between the multi-solid waste material and OPC, a water-cement ratio of 0.6 for OPC can ensure that the material can form a slurry. The water-binder ratio of the multi-solid waste material in Table 3 was controlled at 0.15–0.29, which can ensure that the prepared material can be molded smoothly.

Table 3. The randomly designed mixing proportions of the pastes with diverse solid wastes for the exploration of self-hardening.

No.	Binders (g)									Water (g)	W/B
	CSG	SR	FFAII	FFAI	GBFS	LP	RM	BRS	GP		
D01	100	50	200	50	50	100	50	100	50	200	0.27
D02	100	100	200	100	100	100	100	100	100	200	0.20
D03	200	100	200	100	100	100	100	100	100	200	0.18
D04	200	100	200	200	100	100	100	100	100	200	0.17
D05	200	100	200	100	200	100	100	100	100	200	0.17
D06	200	100	200	100	200	100	100	100	200	200	0.15
D07	50	50	200	50	50	100	50	100	50	200	0.29
D08	50	50	300	50	50	100	50	200	50	200	0.22
D09	50	50	300	50	50	100	50	300	50	200	0.20
D10	50	50	400	50	50	50	50	300	50	200	0.19
D11	50	50	400	50	50	50	50	400	50	200	0.17
D12	50	50	500	50	50	50	50	400	50	200	0.16

Note: W/B is the water-to-binder ratio. Binders is all solid materials. In this case, the OPC paste was likewise produced using 1250 g cement and 750 g water with a W/B ratio of 0.6.

(2) Nine samples for mixing ratio optimization

After that, nine more sample groups were used to investigate the influence of FFAI, GBFS, LP, and RM on fresh and hardened characteristics, hence contributing to the determination of the appropriate mixing ratio. During testing, it was determined that the ratios of FFAI, GBFS, LP, and RM alter the mechanical strength and workability characteristics of backfill pastes; hence, these concentrations were chosen to examine their effects. In addition, the backfill pastes were produced utilizing the same mixing and curing processes as mentioned before. The same amount of water, 250 g, was utilized to achieve fluidity. Table 4 displays the specified proportions for the combinations of backfill pastes ('F*' group). Injecting fresh pastes into cylindrical PVC molds (36 mm in diameter and 36 mm in height). In contrast to the previous experimental findings [41], the selected molds with a height-to-diameter ratio (H/D) of 1:1 are more practical.

Table 4. The designed mixing proportions of the backfill pastes used to assess the physical and mechanical properties, stability, as well as micro-characterization.

No.	Binders (g)											Water (g)	W/B
	CSG	SR	FFAII	BRS	GP	FFAI	LP	GBFS	RM	OPC	NaOH		
F1	50	25	100	25	25	25	50	25	25	—	—	250	0.71
F2-1	50	25	100	25	25	0	50	25	25	—	—	250	0.77
F2-2	50	25	100	25	25	50	50	25	25	—	—	250	0.67
F3-1	50	25	100	25	25	25	50	0	25	—	—	250	0.77
F3-2	50	25	100	25	25	25	50	50	25	—	—	250	0.67
F4-1	50	25	100	25	25	25	25	25	25	—	—	250	0.77
F4-2	50	25	100	25	25	25	75	25	25	—	—	250	0.67
F5-1	50	25	100	25	25	25	50	25	0	—	—	250	0.77
F5-2	50	25	100	25	25	25	50	25	50	—	—	250	0.67
P1	200	100	400	100	100	100	200	100	100	—	—	980	0.70
P2	—	—	—	—	—	—	—	—	—	1400	—	900	0.64
P3	200	100	400	100	100	100	200	100	100	—	200	980	0.61

Note: W/B is the water-binder ratio. The Binders are all solid materials.

(3) Three samples for properties comparison and microstructural characterization

After the effect studies of FFAI, GBFS, LP, and RM, the appropriate mixing ratio of backfill paste with various solid wastes was obtained, and the backfill pastes with high workability were utilized to compare drying shrinkage, permeability, and chemical attack with the OPC paste and alkali-activated paste by NaOH. The backfill pastes were also created utilizing the same mixing and curing procedures as previously. The proportions of the utilized paste samples ('P*' group) are shown in Table 4.

2.3. Testing Methods

2.3.1. Determination of Fresh and Hardened Properties

The pH value, electrical conductivity (EC), fluidity, and setting time of the backfill pastes made from various solid wastes were determined. In addition, the hardened properties, including water absorption, bulk density, and unconfined compressive strength (*UCS*), were measured. In addition, the stability of hardened pastes exposed to severe conditions, such as drying shrinkage, permeability coefficient, and mass and strength changes in response to Na_2SO_4 and NaCl solution attacks, were examined.

Measurement of pH and EC Values

The EC shows the presence of conductive soluble ions and cations, whereas the pH value reflects acid and alkaline characteristics [31]. Raw materials were soaked for 24 h in a 1:5 solid-water ratio in tap water (weighing 20 g total) to determine their pH and EC values. The glass containers were covered at room temperature to prevent water loss. To further evaluate the impact of hardened pastes on environmental water, the pastes were soaked in water and their pH and electrical conductivity (EC) were determined. Hardened samples weighing 30 g were soaked in tap water weighing 150 g (a solid-to-water ratio of 1:5) for 1, 7, and 28 days at room temperature. A DDS-307A conductivity meter was used, which has a resolution of 0.01 mS/cm, a maximum range of 100 mS/cm, and a constant of 10 cm^{-1} for its electrode probe. At least five independent measurements were taken to assure the reliability of the results.

Measurement of Fluidity

To determine the fluidity of the backfill pastes, the flow diameters were measured following ASTM C230/C230 M. The newly synthesized pastes were cast into a slump cone mold (top diameter 36 mm, bottom diameter 60 mm, and height 60 mm) on a glass plate after three minutes of mixing solids and tap water [9,25,26]. The droop cone mold was pulled vertically after scraping the paste off the top surface with a steel ruler. The paste

then flowed freely for 30 s while the steel ruler measured the two maximum diameters in the vertical direction. Using the average of two maximum diameters, the fluidity of fresh paste was calculated. The fluidity test was completed in six minutes, from the adding of water to the measurement of the flow diameter.

Measurement of Setting Time

One of the most important characteristics of binder paste materials is setting time, which is defined as the final time, when the backfill paste initially loses its fluidity, and the final setting time, when its plasticity completely vanishes and strength begins to emerge [42]. Initial and final setting times were measured using Vicat equipment following GB/T 1346-2011 (in China).

Measurement of Water Absorption

The water absorption tests were conducted by ASTM C67-07. Using the Equation (1), the Water absorption (%) was calculated [37]:

$$Water\ absorption = [(W_1 - D_0)/D_0]100\% \quad (1)$$

where W_1 is the weight (g) of the sample after 24 h of soaking in water and D_0 is the weight (g) of the sample after oven-drying.

Measurement of Bulk Density

The ASTM C830-00 method was used to calculate the bulk densities of hardened backfill pastes. The average was determined from three identical samples. Using the following Equation (2) [13,36], the bulk density (g/cm^3) was calculated:

$$Bulk\ density = D_0/V_0 \quad (2)$$

where D_0 and V_0 represent the samples' dry weight (g) and volume (cm^3), respectively.

Determination of Unconfined Compressive Strength (UCS)

The UCS is a significant mechanical performance of a hardened backfill paste that is used to detect whether the backfill paste has been damaged by external force [43]. The UCS of hardened pastes and controls at 28 and 90 days were determined by using an unconfined compressive strength machine (TCQ-10, Kexing Instrument Enterprise, Cangzhou, Hebei Province, China) with a loading strain rate of 1.0 mm/min [44]. The UCSs at 28 and 90 days were chosen to measure because the strength of samples reaches stability after a at longer curing time. The results were determined by calculating the mean of five identical hardened samples. Using the following Equation (3), the UCS result (MPa) was calculated:

$$UCS = M_L/A_0 \quad (3)$$

where M_L denotes the maximum load at failure (N), and A_0 denotes the average bed face area (mm^2).

Determination of Drying Shrinkage

According to the Chinese standard JC/T 603-2004 [45], the pastes were cured at room temperature for one day after being cast in a 25 mm × 25 mm × 280 mm steel mold. At that time, the original lengths of the samples were recorded. The samples were then left at room temperature to cure. The lengths of the samples were measured using a ratio-length meter (BC156-300, Lisheng Instrument Enterprise, Changzhou, Hebei Province, China) with a three-day internal after standard par adjustment. The drying shrinkage values of the samples were measured at 3, 14, 28, 56, and 90 days to calculate the mean of three identical samples.

Determination of Permeability Coefficient

Using a self-made backfill permeability tester, the permeability of the hardened samples was examined. The testing equipment comprises a reading device and a testing device coupled to a device for the high-water supply [9]. The coefficient of permeability was determined using cylindrical samples of 15 cm in diameter and 25 cm in height [9,46]. Again, five identical samples of hardened material were examined for each case, and the average findings were given for the 28-day test results.

Characterizations of Na_2SO_4 and NaCl Solution Attacks

Backfill material for goafs often confront difficult erosive conditions due to subsurface sulfate and chloride, which primarily affects the durability of backfill materials utilizing varied solid wastes as an alternative to OPC paste [8]. Typical attack solutions of 10% Na_2SO_4 solution and 10% NaCl solution in mass concentration were employed to approximate eroding conditions. Moreover, a high mass concentration of the attack solution was used to generate a substantial difference in testing findings, which is more than the mass concentration of 5% reported in earlier studies [47]. Before conducting studies, 30 mm × 30 mm × 30 mm samples [41] were submerged in water for 24 days and their starting weight was determined. Then, Na_2SO_4 and NaCl attack studies were conducted by immersing the samples for 90 days in 10% Na_2SO_4 and 10% NaCl solutions, respectively. During that time, the glass containers were filled with a volume ratio of 1:1 for solids to liquids. The Na_2SO_4 and NaCl attack performances were evaluated using changes in mass and UCS [47], which were continuously recorded with submerged age up to 90 days with a 30 days interval. To limit moisture loss and solution concentration's impact, plastic sheets were used to cover the glass container. To sustain the severity of the erosion, the attack solutions were changed every fifteen days. To calculate the mass and UCS, the average of five identical samples was used.

2.3.2. Microstructures, Products, and Thermal Stabilities of Hardened Pastes

The SEM-EDS tests were used to analyze the micro-characteristics and reveal the cementation method of the best backfill paste (P1) with various solid wastes in comparison to those of raw materials. Using SEM-EDS, the morphology, microstructure, and elemental components of 90-d samples (P1) were compared to those of raw materials. The EDS spectra were collected to analyze the elemental distributions of various phases. With energy dispersive spectroscopy, a scanning electron microscope (SEM-EDS, Quanta FEG450, FEI, Hillsboro, OR, USA) was used.

Additionally, the XRD patterns were analyzed to show the crystal and amorphous phases of the backfill paste P1 [10,37]. The FTIR examinations on 90-d samples were performed. The testing parameters are described below: a scanning range of 10°–80° 2θ and a scanning rate of 2°/min. When the paste was cured for 90 days, X-ray diffraction spectroscopy (XRD, D/MAX-2500, Rigaku, Japan) was employed to determine the mineral compositions.

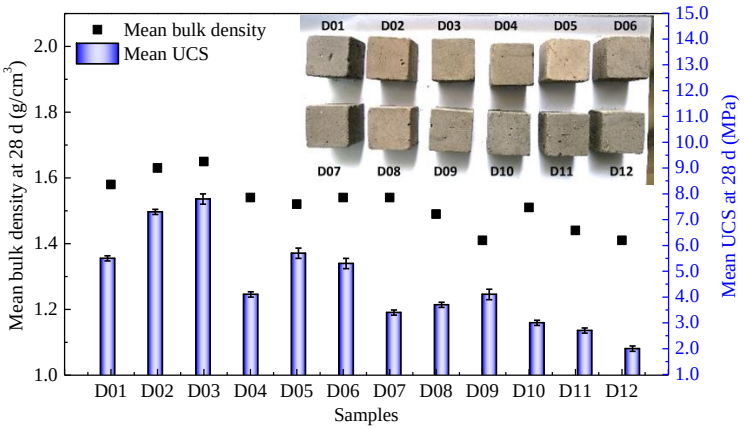
The FTIR spectra were acquired to further investigate the product alterations from the typical vibration peaks of chemical bonds [48]. The FTIR examinations on 90-d samples were performed. Before being crushed into powders, the samples were air-dried for 48 h. The powders (1.3 ± 0.001 mg) were then combined with potassium bromide (KBr) pellets to create the tested specimens (weighed 130 mg). Fourier transformation infrared spectroscopy was employed to investigate the wavelength range of 500 to 4000 cm^{-1} (FTIR, Nexus 8, Bruker, Karlsruhe, Germany).

Thermo-Gravimetric/Differential Thermal Synchronous Thermal Analysis Spectrometer (TG-DSC) tests on the backfill paste (P1) with solid wastes were conducted using a STA449F5 thermal analyzer (NETASCH, Selb, Germany), which also helps to verify the products according to the thermal decomposition caused by phase changes. The entire weight of the sample was 8.00 mg, and the testing temperature ranged from 30 °C to 1000 °C. The air environment was used following a heating rate of 15 °C/min.

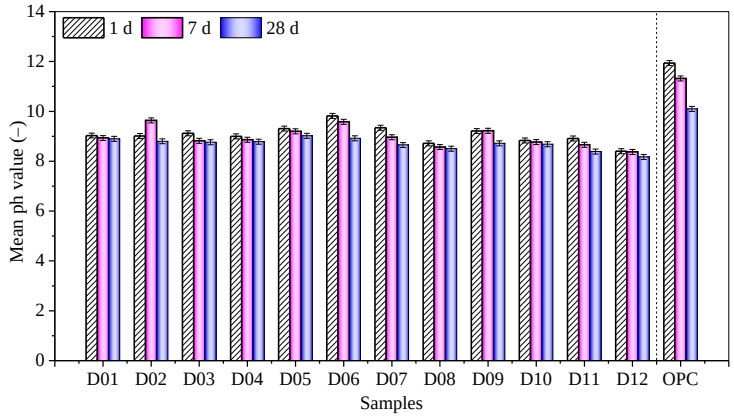
3. Results and Discussion

3.1. Self-Hardening and Alkali Seepage of Pastes

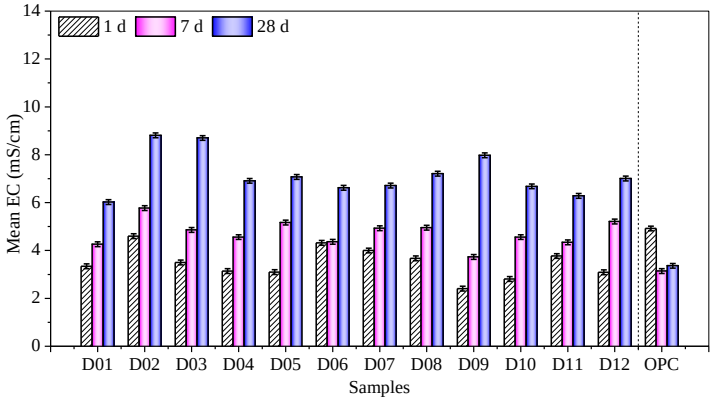
As shown in Figure 1, the 28-d UCS and bulk density were used to evaluate the self-hardening of the backfill paste derived from diverse solid wastes (Figure 1a), and the pH and EC were measured to analyze the effects of the hardened backfill pastes on the environments after different immersion ages of 1, 7, and 28 d (Figure 1b,c).



(**a**)



(**b**)



(**c**)

Figure 1. The results of (**a**) 28-d UCS and bulk density of hardened pastes derived from diverse solid wastes together with (**b**) pH and (**c**) EC of environmental water. Note: 'OPC' means the compared cement paste with a water-cement ratio of 0.6. pH = 7.40 and EC = 80.00 μS/cm for the initial tap water.

After the raw materials were blended with water, the 28-d UCS of the hardened backfill paste reached a range of 2.0–7.8 MPa, with sample D03 having the highest 28-d UCS of 7.8 MPa (Figure 1a). The 28-d UCSs of the synthesized pastes satisfy the required mechanical properties for backfill grouting materials for goaf use (the required 28-d UCS should reach higher than 0.6 MPa [36]). Additionally, the bulk densities of hardened pastes ranged 1.41–1.65 g/cm^3 (Figure 1a). The best self-hardening results in the highest 28-d UCS were 7.8 MPa and the maximum bulk density of 1.65 g/cm^3. Due to the high 28-d UCS, the hardening effect of the backfill paste with diverse solid wastes is similar or even superior to other reported backfill materials such as alkali-activated FA-based and FA-SR-based paste materials for goaf backfill [36,49].

Furthermore, the impacts of hardened pastes on the environment were studied by using pH and EC measurements. When hardened pastes were immersed in water for 28 days, the environmental waters had an alkaline pH range of 8.17–9.02 and an EC range of 3.08–8.81 mS/cm based on the different mixing proportions of hardened pastes (Figure 1b,c). The alkaline pH values of environments with diverse solid wastes were lower than that of OPC paste (pH = 10.10), while the ECs of environments were higher than that of OPC paste (EC = 3.36 mS/cm). The environmental pH and EC are directly connected to the alkalinity of raw materials and the soluble cations and ions [31]. The measured ECs of paste containing diverse solid wastes were higher than those of OPC paste due to more soluble ions and cations dissolved in the environment water.

The pH values of environmental water fell slightly and the EC increased dramatically as the immersion age increased from 1 day to 28 days. These were associated with the chemical alkali-activated reaction as well as ion and cation physical absorption [50]. The hardened pastes were immersed in water (initial pH was 7.40 and initial EC was 80.00 mS/cm), and soluble ions and cations on the sample surface were released into the surrounding water, resulting in greater pH and EC values. After that, the pastes continued to form hydrated and geopolymerized product gels to absorb some soluble ions and cations such as Ca^{2+}, Na^+, and OH^- from the environment, resulting in slightly decreased pH values with immersion age [8,23,51].

As a consequence, it is possible to prepare self-hardening backfill pastes from diverse solid wastes (including CSG, SR, RM, GBFS, FFAI, FFAII, and BRS), and the backfill pastes have less impact on the underground environment than the OPC paste in alkaline pH values. Additionally, one-step mixing preparation of backfill pastes is more convenient and achievable by directly adding water into solid mixtures without the introduction of strong alkaline activators such as NaOH and Na_2SiO_3.

3.2. Effects of Raw Materials on Fresh and Hardened Properties

After the self-hardening verification of the pastes, the effects of raw material dosages on fluidity and 28-d UCS were investigated, as seen in Figure 2.

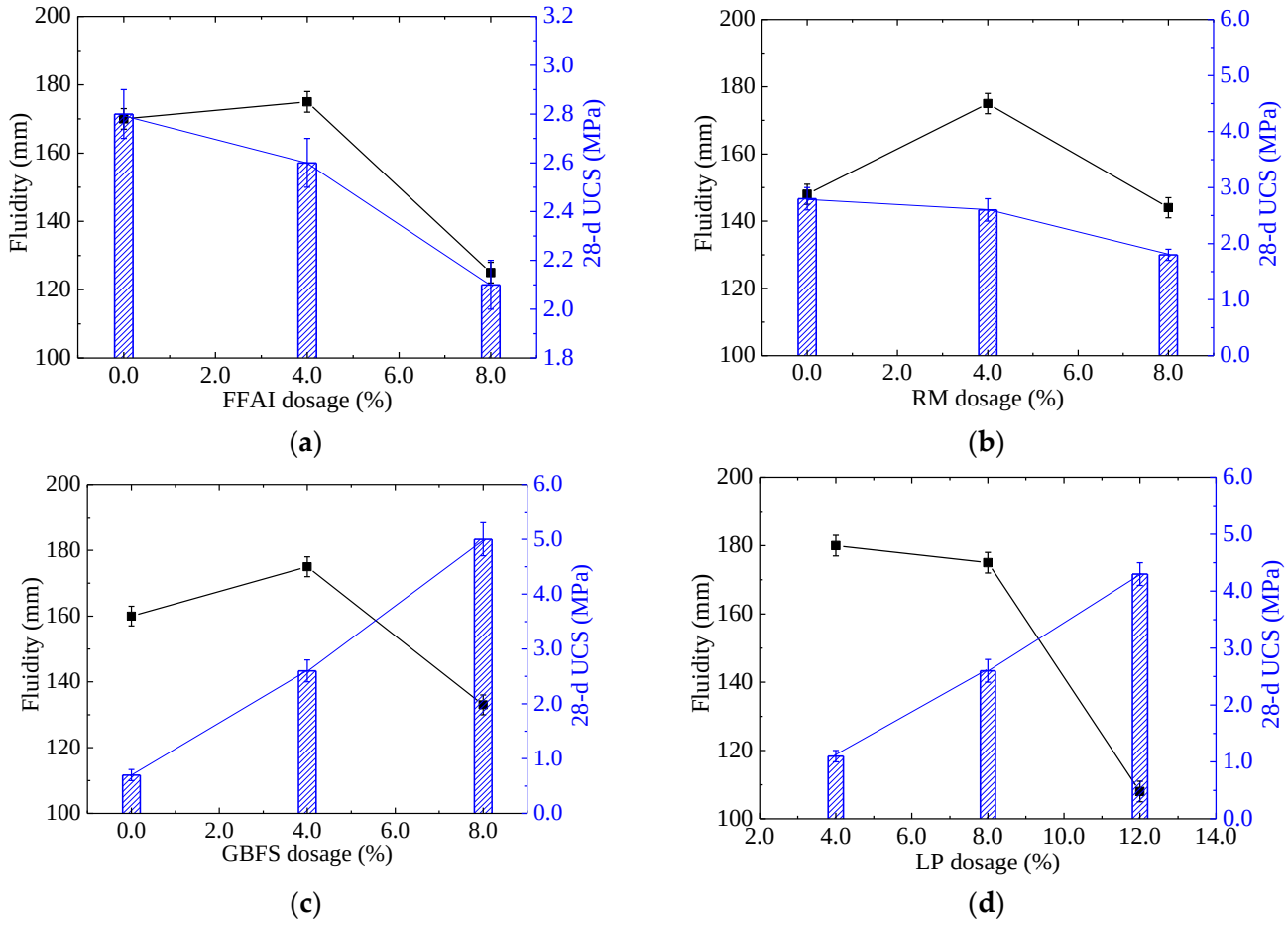


Figure 2. The influence of raw material dosages on average fluidity and 28-d UCS of the backfill pastes. (**a**) FFAI, (**b**) RM, (**c**) GBFS, and (**d**) LP.

Regarding low-calcium silica-alumina precursors, the addition of FFAI and RM exhibit identical trends in fluidity and 28-d UCS with dosage increase, showing that the 28-d UCS decreases by 25.0% and 35.7%, respectively, with an increase in FFAI dosage from 0.0% to 8.0% and RM dosage from 0.0% to 8.0%, as seen in Figure 2a,b. The decreased 28-d UCS is attributable to the slower reactivity with increased FFAI and RM concentrations in the system under alkaline conditions [6,52]. Furthermore, when FFAI and RM dosages increase, the fluidities of backfill paste first increase and subsequently decline. Regardless of the low water absorption of FFAI and RM, the change in fluidity results from early chemical bonding between generated product gels and physical rolling between unreacted spherical particles [26]. The fluidity is highest by the combined effects of chemical bonding and physical rolling at FFAI dosages of 4.2% and RM dosages of 4.2%, respectively. It demonstrates that FFAI and RM have a major impact on fluidity and 28-d UCS.

There is an identical growing tendency of 28-d UCS in terms of high calcium and high reactivity of GBFS as well as high-calcium-based additive LP, as illustrated in Figure 2c,d, respectively. This reveals that increasing the GBFS dosage from 0.0% to 8.0% and the LP dosage from 4.4% to 12.0% enhances the 28-day UCS by 6.1 and 2.9 times, respectively. Higher cementations of the formed product gels primarily determine the greater 28-d UCS of backfill pastes, and higher cementations may also be supplied by more product gels from GBFS and LP, which should be confirmed further by microscopic testing techniques. Additionally, higher GBFS and LP dosages result in lower backfill paste fluidities, which coincides with the workability conclusion of GBFS-based geopolymer backfill paste reported in the previous literature [2,53]. The fluidity decrease is mainly due to the high water-absorption and rapid hydration reaction of GBFS and LP when the raw materials

are combined with water to form new pastes. The effects of two different FAs and lime on the development of compressive strength as well as the hydration reaction of FA/GBFS mixes that had been activated by NaOH and Na_2SiO_3 solutions were examined by Shi and Day [54]. In addition to this, they discovered that the early UCS of alkali-activated materials may be substantially enhanced by the addition of a little quantity of lime.

As a result, the FFAI, RM, GBFS, and LP dosages should be properly regulated to meet the requirements of fluidity and 28-d UCS for the backfill pastes. These conclusions are critical for determining the optimal mixing proportions for backfill paste using diverse solid wastes.

According to the reports below, the functions of FFAII, CSG, BRS, SR, and GP were also revealed. Despite different particle sizes, FFAII had a similar influence on fluidity and 28-d UCS as FFAI due to the same components and surface properties. In terms of CSG, increasing the CSG/GBFS ratio produces more crystal calcium hydroxide, which is detrimental to strength development, while adding LP offers more $Ca(OH)_2$ than CSG to accelerate GBFS hydration [2]. Previous research found that the addition of 20.0% CSG to FA-based geopolymer composites decreased fluidity and improved long-term strength [7]. Owing to their identical chemical components after the burning process, BRS should possess similar effects on the characteristics of pastes as CSG. Furthermore, the appropriate amount of SR was introduced to the FA-based geopolymer paste to enhance the properties of the paste mixture for goaf backfill. According to the range analysis, the fluidity and 28-d UCS values rose and subsequently dropped as the SR-FA ratio increased, with the maximum fluidity and strength occurring at an SR-FA ratio of 2:3 [9]. Following that, 10% GP was employed as a replacement to Na_2SiO_3 in SR-FA-based geopolymer paste for goaf backfill, with a high fluidity of 196–222 mm and an appropriate 28-d UCS of 0.92 MPa [36]. It was concluded that 10% GP effectively improved fluidity and UCS thereby meeting the performance requirements of goaf backfill material.

Therefore, each raw material adopted in this paper possesses the effects of improving the workability and mechanical strength of backfill pastes in chemical and physical aspects; However, it is essential when determining the role of each raw material to obtain the optimal mixing properties of the backfill paste.

3.3. Performance Assessment of Shrinkage, Permeability, and Chemical Attack

3.3.1. Determination of the Optimal Mixing Proportion of Backfill Paste

To meet the property requirements of backfill paste for goaf, the backfill paste was further optimized. The best mixing proportions of the backfill paste, as determined by experiments, were as follows: water-binder ratio of 0.70; density, 1500 kg/m^3; 7.14% FFAI; 28.57% FFAII; 7.14% RM; 14.29% CSG; 7.14% SR; 7.14% GBFS; 7.14% BRS; 14.29% LP; and 7.14% GP by mass. As shown in Figure 3, the backfill paste P1 outperformed the OPC paste P2 in terms of fundamental performance. In addition to having a fluidity of 201 mm, it satisfied all the property requirements of backfill paste by having an initial setting time, a final setting time, and a UCS of 28 days. Moreover, solid NaOH pellets were added to the backfill paste in sample P3 to serve as a reference sample. Sample P1 had better workability than sample P3, the same UCS (28 days), but shorter initial and final setting times. Then, compared to P3 and P2, P1 had less impact on the environment in terms of pH and EC. Hence, the optimal mixing proportion of backfill paste employing diverse wastes was determined, allowing for further performance assessment of the drying shrinkage, permeability, and chemical attack, as shown in Figure 4.

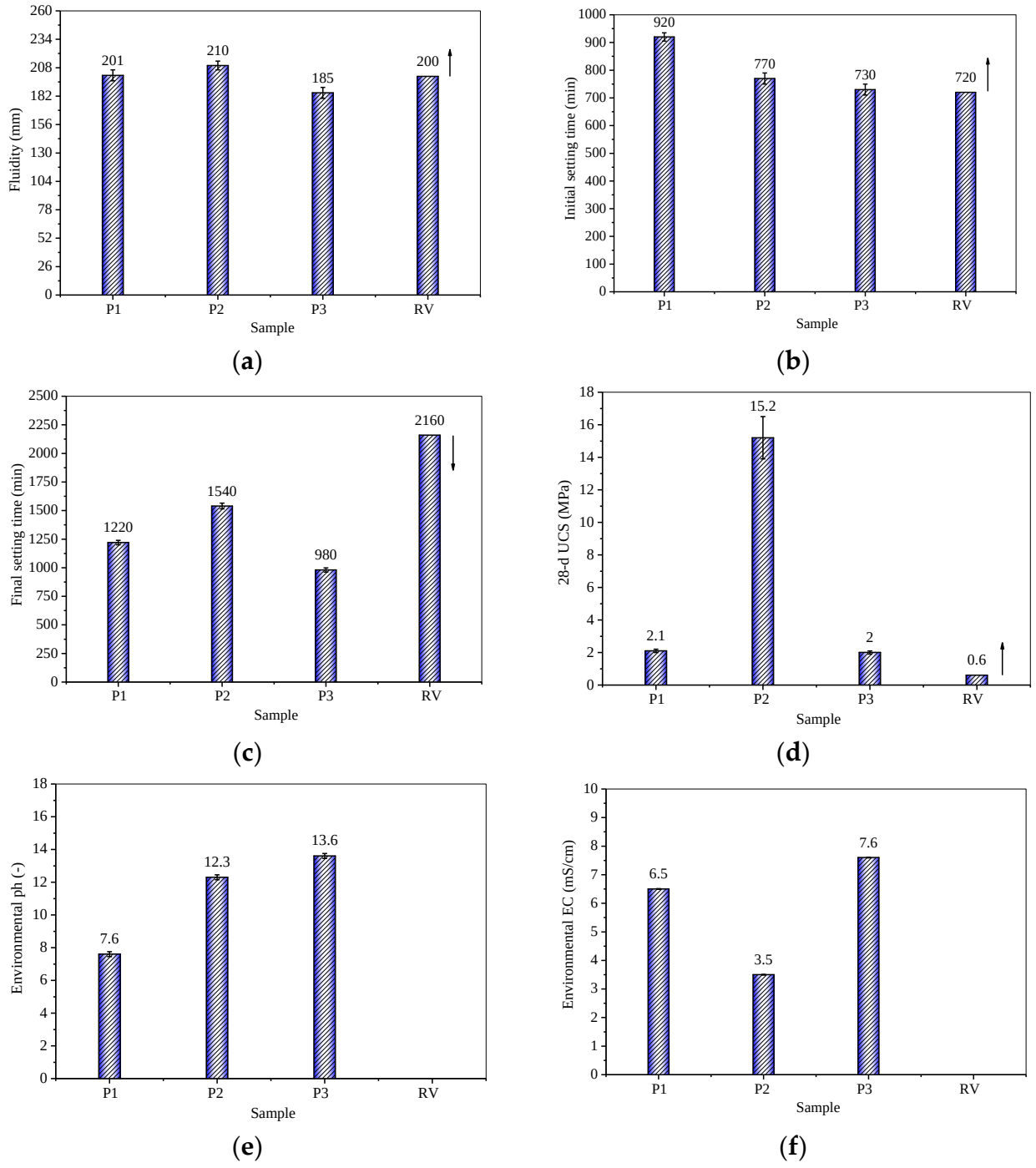
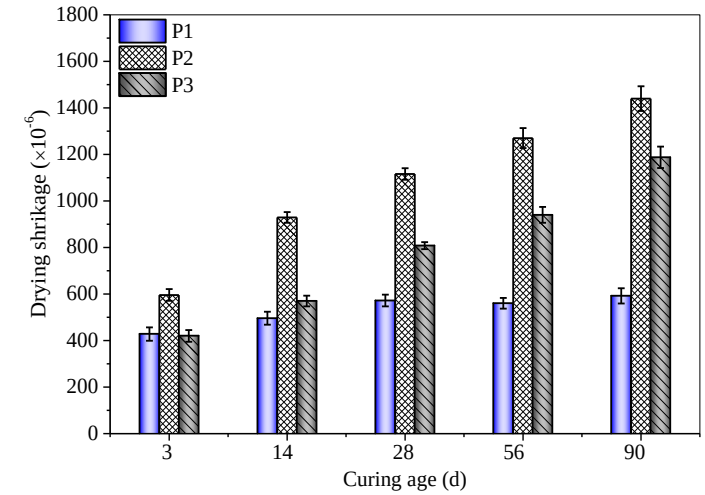
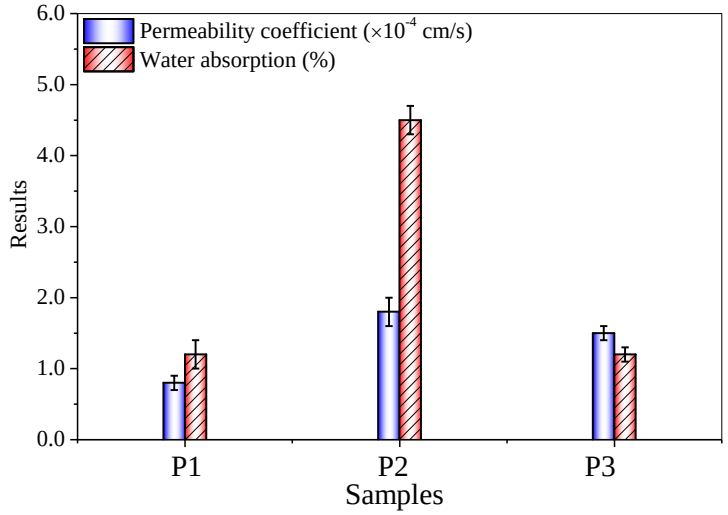


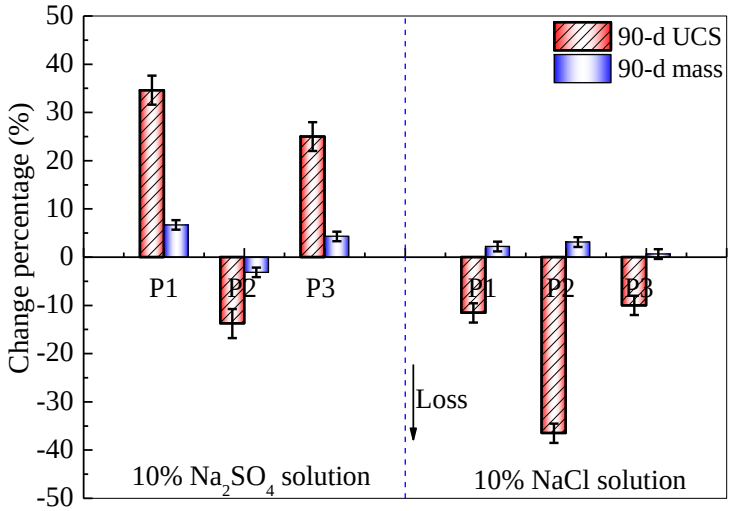
Figure 3. The performance of the optimal backfill paste P1 made from diverse solid wastes compared to control samples P2 and P3. (**a**) Fluidity, (**b**) initial setting time, (**c**) final setting time, (**d**) 28-d UCS, (**e**) environmental pH, and (**f**) environmental EC. Herein, the required value (RV) refers to the basic engineering requirement for OPC paste. Here, '↑' denotes a required higher value and '↓' refers to a required lower value than RV.



(**a**)



(**b**)



(**c**)

Figure 4. (**a**) The drying shrinkage, (**b**) the permeability coefficient and water absorption, and (**c**) the mass and UCS under 10% Na_2SO_4 and 10% NaCl solution attack for samples P1, P2, and P3.

3.3.2. Drying Shrinkage Analysis

Figure 4a shows the drying shrinkage results of samples P1, P2, and P3 after 90 days of curing. Under the premise of about 200 mm fluidity, the drying shrinkage values of P1, P2, and P3 rose with curing age up to 90 d at room temperature. Additionally, the 90-day drying shrinkage for P1 reached 592 $\times$ 10^{-6}, 1440 $\times$ 10^{-6} for P2, and 1188 $\times$ 10^{-6} for P3. It shows that the 90-day drying shrinkage value of the backfill paste (P1) with various solid wastes was lower than that of the OPC paste (P2), and lower than that of the paste P3 activated by NaOH pellets.

The GBFS, CSG, and SR play different roles in improving the drying shrinkage of the paste owing to their calcium-containing chemical components and chemical nature. Shang et al. [28] reported that the addition of 20.0% GBFS increased the drying shrinkage of FA-based geopolymer material due to its rapid hydration nature and large water absorption. Furthermore, the addition of 20.0% CSG led to a decreasing trend in the drying shrinkage of FA-based geopolymer material due to the main composition of $Ca(OH)_2$ and CaO [7]. In addition, the 20.0% SR reduced the shrinkage of FA-based geopolymer material owing to the chemical compositions of insoluble $CaCO_3$, $CaSO_4$, and $Ca(OH)_2$ in SR [13]. Previous works found that FA-based geopolymer showed lower shrinkage than that of the OPC [53,55], while alkali-activated GBFS-based material exhibits a larger shrinkage than that of OPC [56]. As a result, the used high-calcium-based waste slags, and low-calcium silica-alumina precursors completely show their advantages in combination with additives to obtain lesser shrinkage of the prepared backfill paste P1 with various solid wastes. It is confirmed that the backfill paste P1 possesses a better drying shrinkage-resistant behavior than the OPC paste owing to the positive influences in the chemical composition and nature of industrial solid wastes.

3.3.3. Permeability Coefficient Analysis

The permeability coefficients are shown in Figure 4b. Sample P1 has a permeability coefficient of 0.8 $\times$ 10^{-4} cm/s and a water absorption of 1.2%, while the OPC paste (P2) has a permeability value of 1.8 $\times$ 10^{-4} cm/s and a water absorption of 4.5%. Additionally, the permeability coefficient of P3 is 1.5 $\times$ 10^{-4} cm/s, with a water absorption rate of 1.2%. The higher water absorption of the OPC paste P2 is due to the hydration process [21], which requires water to serve as a reactant during curing. The lower permeability coefficient of P1 may be attributed to the diverse product gels of C-A-H, C-S-H, C-A-S-H, and N-A-S-H gels, etc., but this needs to be verified further using SEM-EDS, XRD, and FTIR techniques. When NaOH pellets were mixed with various solid wastes, the permeability coefficient of P3 was higher than that of P1. It illustrates that independent of water absorption, the addition of NaOH pellet had a detrimental influence on permeability due to the obstruction of hydration induced by excessive strong alkalinity and the lower structural compactness caused by uneven contact between particles in the paste [22,37].

3.3.4. Changes in Mass and UCS under Sulfate and Chloride Attack

Figure 4c depicts the mass and UCS changes of pastes P1, P2, and P3 at different attack ages. Samples P1 and P3 exhibited increases in mass and UCS after 90 days of Na_2SO_4 solution attack, while the OPC paste (P2) shows losses in mass and UCS. This demonstrates that the backfill paste containing various solid wastes is more resistant to Na_2SO_4 solution attack than the OPC paste. It may be because the generated mixtures of N-A-S-H and C-S-H gels in the backfill paste P1 have lower water absorption than OPC paste [37], and those product gels continue to generate under the attack of Na_2SO_4 solution [8]. After 90 days of Na_2SO_4 solution attack, P2 was eroded by Na_2SO_4, resulting in mass and UCS losses due to the chemical reaction between Na_2SO_4 and C-S-H in OPC to generate calcium sulfate ($CaSO_4$) crystals and ettringite (AFm) [42,47]. However, the mass and UCS of P1 and P3 both increased with attack age. It is because environmental Na+ cations diffuse into the network microstructure of geopolymeric Si-O-Al chains and have a beneficial influence on

the polymerization degree of Si-O-Al chains [57]. After a Na_2SO_4 attack for 90 days, the mass of P1 increased by 6.67%, and the UCS increased by 34.62%.

Under NaCl solution attack for up to 90 d, P1, P2, and P3 present a loss in UCS, while an increase in mass is due to the introduction of Na^+ with attack age. Moreover, the UCS loss and mass loss of P1 are lower than that of P2, which is determined by the product gels in the backfill paste. Because the alkali-activated product gels suffer from negligible NaCl solution erosion, P3 has close mass and UCS losses to P1. After 90 days of NaCl attack, the mass of P1 rose by 2.20% while the UCS decreased by 11.54%. Although many factors influenced the behavior and reaction of alkali-activated GBFS, such as chemical composition, type, and concentration of activators, curing temperature, etc., alkali-activated GBFS-based materials were reported to have better durability in an aggressive environment than OPC, particularly high resistances to sulfates and chlorides [21,58]. Furthermore, many investigations have demonstrated that alkali-activated GBFS-based materials have strong resistance to chloride ion penetration and very low chloride diffusion due to low calcium content and permeability [59,60]. As a result, the paste P1 containing GBFS outperformed the OPC paste in terms of resistance to Na_2SO_4 and NaCl solution attacks.

3.4. Morphology and Microstructure Analysis of Hardened Paste by SEM-EDS

The SEM images were used to evaluate the morphologies of raw materials (Figure 5). The FFAII's primary morphology consists of spherical glass beads and irregular particles, similar to FFAI's spherical glass beads. After high-temperature burning, the primary glass beads are created by fast cooling [6,30]. The RM, CSG, GBFS, BRS, and LP have flaky, block and other particle morphologies with scattered structural characteristics [33–35,61], while the GP has an agglomerated structure. In addition, SR is composed of round, flaky, and hazy particles and has an agglomerated and loose structure. The observations of SEM images corroborates those of previous observations of SR [8,9,13,22]. Particularly spherical and granular ingredients enhance the fluidity of backfill pastes before dissolution [36,49,62]. In addition, all raw materials have potential reactivity in alkaline circumstances [63,64]. The FFAI, FFAII, RM, and GBFS display potential alkaline hydration and geopolymerization reactivity. The formation of layered C-S-H, C-A-H, and C-A-S-H gels is governed by the chemical reaction of CaO, $Ca(OH)_2$, and silica-alumina components [65]. Geopolymerization, on the other hand, is the consequence of a chemical polymeric interaction between Al-O and Si-O bonds associated with the cations Na^+ and Ca^{2+}, etc., to create sodium aluminosilicate gel (N-A-S-H) and calcium-containing sodium aluminosilicate gel (N,C)-A-S-H [6,13,65]. The glassy SiO_2 and Al_2O_3 in FFAI, FFAII, RM, and GBFS were typically dissolved and subsequently geopolymerized to generate aluminosilicate polymeric gels [62,66,67]. The calcium used in most synthetic compounds comes from GBFS as well. Nevertheless, others, particularly calcium sources like GP, LP, SR, CSG, and BRS, show potential reactivity upon hydration due to the presence of the effective chemical components CaO and $Ca(OH)_2$. Because of this, product gels formed by raw materials provide chemical cementation between particles during hydration and geopolymerization [10,22,66].

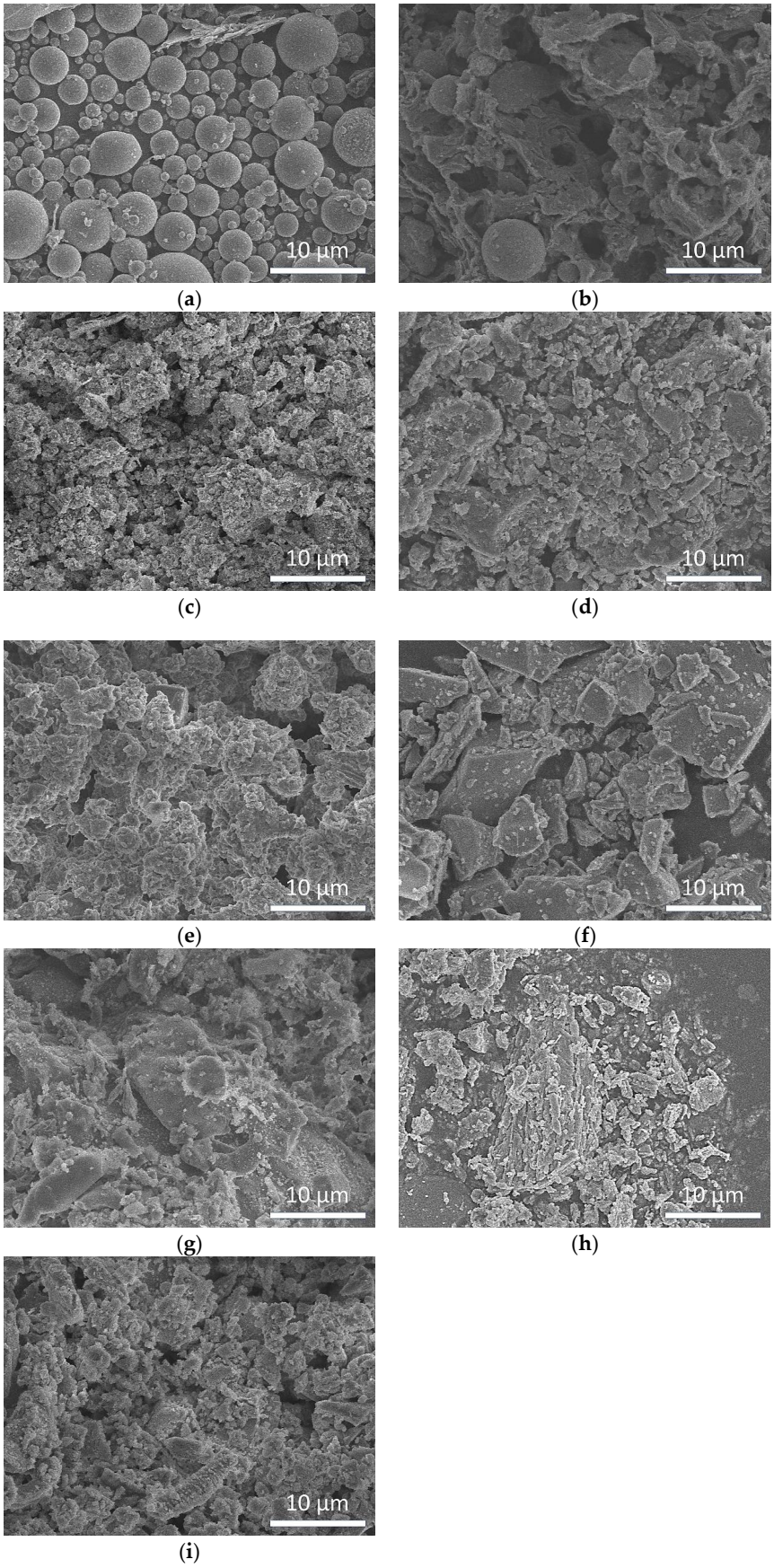


Figure 5. The SEM images of raw materials. (**a**) FFAI, (**b**) FFAII, (**c**) RM, (**d**) CSG, (**e**) SR, (**f**) GBFS, (**g**) BRS, (**h**) GP, and (**i**) LP.

Figure 6 shows the SEM images and EDS spectra of sample P1. With flocculent, the unreactive particles in P1 were encased in the more cementitious material (Figure 6a). In addition, the gels of P1 have a flocculent shape. The flocculent cementation product from P1 was subjected to an EDS spot test (Figure 6b), and the results were the same for both sites (spot 1 and spot 2): the elements O, Si, Al, and Ca predominated, and only a small number of elemental impurities, including Fe and Cl, were not present (Figure 6c,d). The outcome of the cementation is thus most likely a gel composed of C-S-H and/or C-A-S-H. This substance was produced as a byproduct of a process in which P1 lime powder and silica-alumina precursors were subjected to hydration.

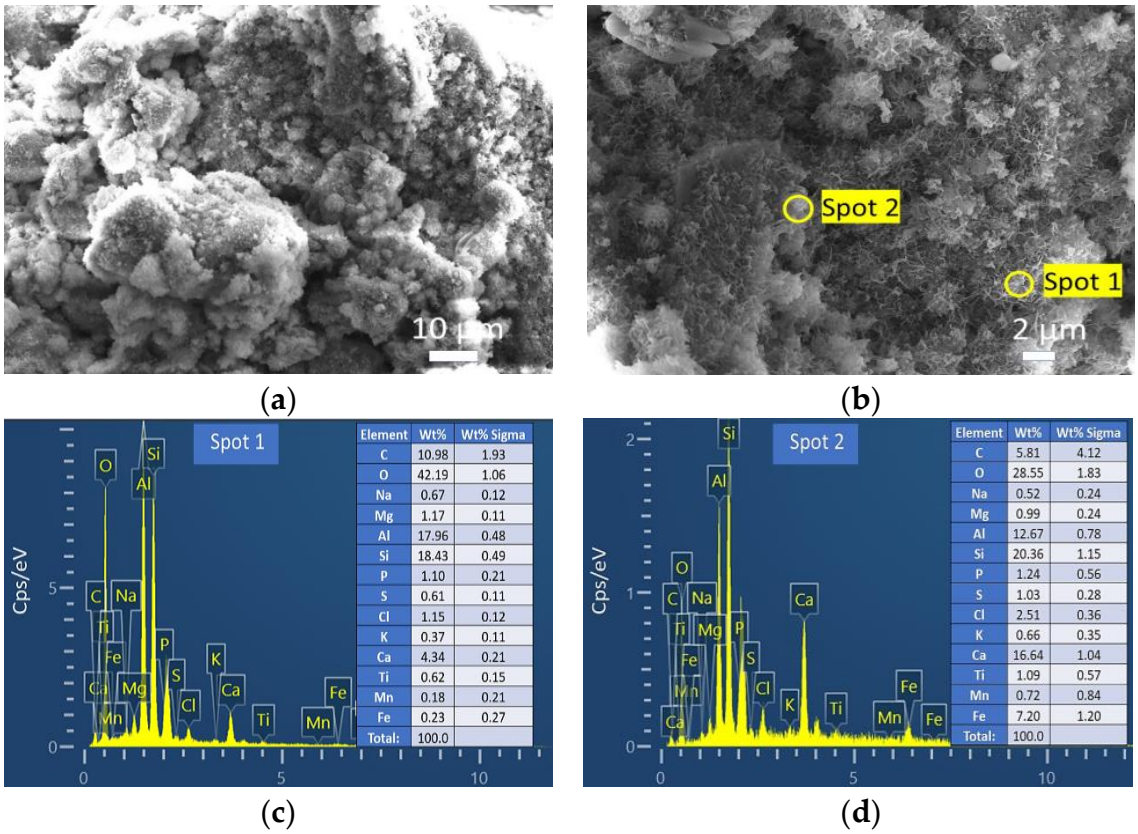


Figure 6. The SEM images of the backfill paste (P1) cured for 90 days. (**a**) ×1000, (**b**) ×3000. The EDS spectra of (**c**) Spot 1 and (**d**) Spot 2.

Figures 5 and 6 are closely related. They are combined to characterize the micromorphological characteristics of the backfill material before and after the reaction. Through the above analysis, it can be proved that the provided various solid wastes can be cemented and have a good hydration and polymerization hardening effect.

3.5. Mineral Components and Chemical Products Analysis of Hardened Paste by XRD and FTIR

Figure 7 shows the XRD pattern of paste P1 and Figure 8 displays the FTIR spectrum of P1. Both were used to reveal the mineral components and chemical products.

The XRD pattern (Figure 7) shows the mixing of amorphous and crystal phases. Amorphous products are essentially the superposition of all amorphous humps in FAI, FAII, BRS, and CS [68], as well as novel amorphous products assigned to wide humps at 18°–40° 2θ. The intensity and angle center of wide humps are affected by the inclusion of amorphous SiO_2 and Al_2O_3, as well as the production of additional amorphous products. Further testing procedures are necessary as XRD patterns do not disclose the precise amorphous compositions of cementitious products designated as C-S-H or (N,C)-A-S-H gels, etc. According to the observed XRD patterns, the P1 contains $Ca(OH)_2$, gypsum,

mullite, quartz, calcite, halite, C-A-S-H, C-S-H, and zeolite crystal compositions. The weakly crystalline C-S-H is accounted for by a high peak at 29°–30° 2θ [69,70], and C-A-S-H is observed at the reflection of 54°–56° 2θ and is related to the poorly crystalline C-S-H and C-A-S-H [2]. The high intensity of C-A-S-H at the reflection of 54°–56° 2θ in P1 accounts for the addition of LP. This is because the addition of LP allows for a higher hydration degree to be produced. In addition, zeolite crystals can be found in P1. In an alkaline environment, amorphous SiO_2 and Al_2O_3 are broken down and geopolymerized to form aluminosilicate gels, which, given the appropriate conditions, crystallize into the zeolite. Aluminosilicate gels are hypothesized to be the precursors of crystal zeolite [71]. Consequently, the XRD patterns show that the 90-d products for the backfill paste P1 and other crystal phases contain a combination of C-S-H, C-A-S-H, and geopolymeric gels. The precise amorphous phases, however, need to be defined further.

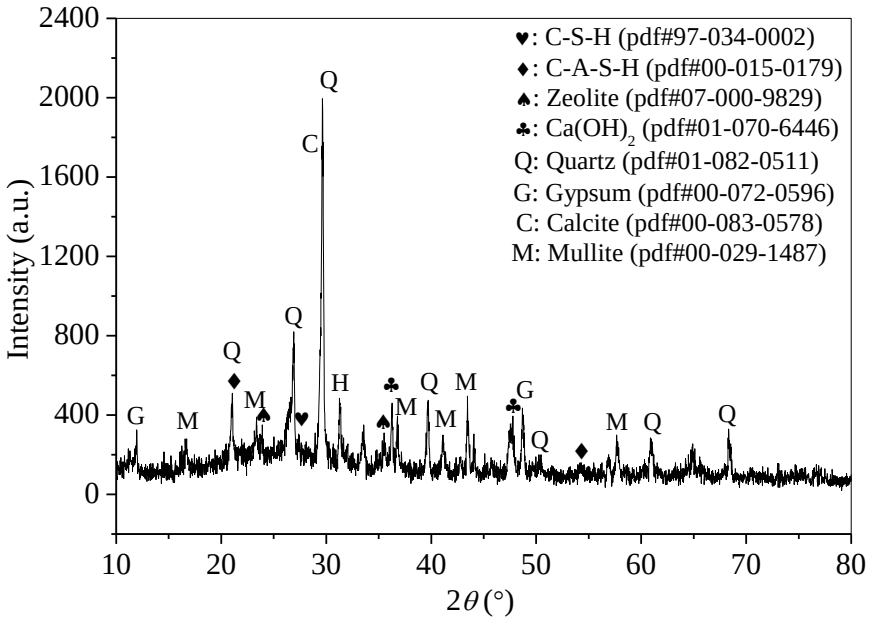


Figure 7. The XRD patterns of the backfill paste (P1) cured for 90 days.

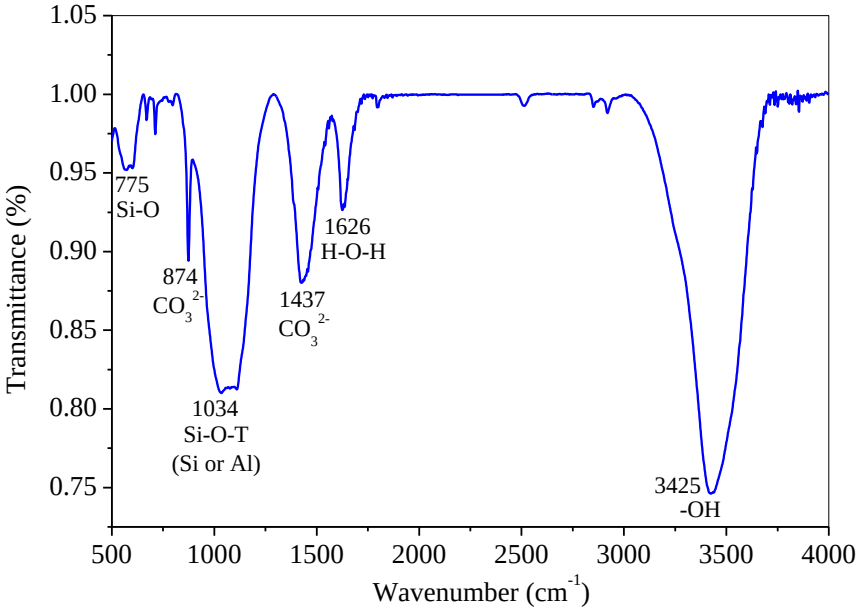


Figure 8. The FTIR spectra of the backfill paste (P1) cured for 90 days.

In Figure 8, the absorption peaks at 3425 cm^{-1} are thought to be caused by the stretching vibration of the OH bonds that are present in H_2O in the FTIR spectrum [36,72], while the absorption peaks at 1626 cm^{-1} are thought to be caused by the bending vibration of the H-O-H bonds that are present in water [8,57]. These absorption peaks show that moisture was present in partly oven-dried materials during specimen preparation. The raw materials FFAI, FFAII, BRS, CSG, GBFS, and RM comprise Al-O-Si chains, which are related to the silica-alumina phase absorption peaks around 960–1100 cm^{-1} and have the potential reactivity to dissolve in alkaline conditions [73,74]. This is also the case due to the fact that these raw materials are produced via the use of high-temperature combustion. Nevertheless, LP, GP, and SR have calcium sources such as $CaCO_3$ and $CaSO_4$ at 1437 cm^{-1} peaks [10,75], as well as $CaCO_3$ at 874 cm^{-1} peaks [10,76]. The FTIR spectra show that the raw materials are suitable for creating backfill paste in both the probable silica-alumina phase as well as the calcium supply. The high absorption peaks at 1034 cm^{-1} from Si-O-Si and Si-O-Al bonds also show the coexistence of hydrated gel C-S-H, C-A-S-H and geopolymer gel (N,C)-A-S-H with a combination of XRD and SEM analysis results. This occurs because the addition of RM causes a rise in the pH of the mixture and supplies the reactants required for the formation of the silica-alumina phase. In more strongly alkaline circumstances, a larger silica-alumina phase composition is favorable for geopolymerization, which ultimately leads to the formation of (N,C)-A-S-H geo-polymer gels containing Na^+ and Ca^{2+} cations [29]. Thus, the hydration process is represented by Equations (4) and (5) reported in previous work [24,37], and geopolymerization by Equations (6) and (7) [6,9,24]. The reaction parameters are x, y, m, and n. According to the findings of the study, the product gels in the backfill paste P1 are in fact a combination of (N,C)-A-S-H gels with C-S-H and C-A-S-H gels. This determines the chemical adhesion of the backfill paste P1 utilizing various types of industrial solid wastes.

$$x\mathrm{Ca(OH)_2} + \mathrm{SiO_2} + (n\text{-}x)\mathrm{H_2O} \rightarrow x\mathrm{CaO{\cdot}SiO_2{\cdot}}n\mathrm{H_2O}\ \text{[C-S-H]} \quad (4)$$

$$x\mathrm{Ca(OH)_2} + y\mathrm{Al_2O_3} + \mathrm{SiO_2} + (n\text{-}x)\mathrm{H_2O} \rightarrow x\mathrm{CaO{\cdot}}y\mathrm{Al_2O_3{\cdot}SiO_2{\cdot}}n\mathrm{H_2O}\ \text{[C-A-S-H]} \quad (5)$$

$$\begin{gathered} m(\mathrm{Si_2O_5},\ \mathrm{Al_2O_3}) + 2m\mathrm{SiO_2} + 4m\mathrm{H_2O} + (\mathrm{Na^+},\mathrm{K^+},\mathrm{Ca^{2+}}) + \mathrm{OH^-} \\ \rightarrow (\mathrm{Na^+},\mathrm{K^+},\mathrm{Ca^{2+}}) + m(\mathrm{OH})_3\text{-Si-O-Al}^-(\mathrm{OH})_2\text{-O-Si-}(\mathrm{OH})_3 \end{gathered} \quad (6)$$

$$\begin{gathered} m(\mathrm{OH})_3\text{-Si-O-Al}^-(\mathrm{OH})_2\text{-O-Si-}(\mathrm{OH})_3 + (\mathrm{Na^+},\mathrm{K^+},\mathrm{Ca^{2+}}) + \mathrm{OH^-} \\ \rightarrow 4m\mathrm{H_2O} + (\mathrm{Na^+},\mathrm{K^+},\mathrm{Ca^{2+}})\text{-[Si(OH)}_2\text{-O-Al}^-(\mathrm{OH})_2\text{-O-Si-(OH)}_3\text{-O-]}_m\ \text{[(N,C)-A-S-H]} \end{gathered} \quad (7)$$

3.6. Thermal Decomposition by TG-DSC Analysis

As shown in Figure 9, the TG-DSC curves of pastes P1 were further obtained along with the DTG curves to analyze the thermal decomposition under high temperatures and determine the products. There are two significant endothermal peaks at 126.33 °C and 731.30 °C. The weight loss of 4.76% due to the decomposition of C-S-H and C-A-S-H with the release of interlayer water and free water corresponds to the endothermal peak at 126.33 °C [77]. Moreover, the endothermal peak at 731.30 °C represents the decomposition of calcite ($CaCO_3$), and a weak peak at 356.40 °C represents the decomposition of aragonite ($CaCO_3$). Both have a weight loss of approximately 16.75%. The presence of $CaCO_3$ is consistent with the XRD patterns. It can be seen that no crystallization of the geopolymer gel into zeolite occurs at 650–720 °C from the TG-DSC curve, which is attributed to the small amount of zeolite content in P1. The hydrated products are mostly amorphous and crystalline C-S-H and C-A-S-H, as well as amorphous (N,C)-A-S-H.

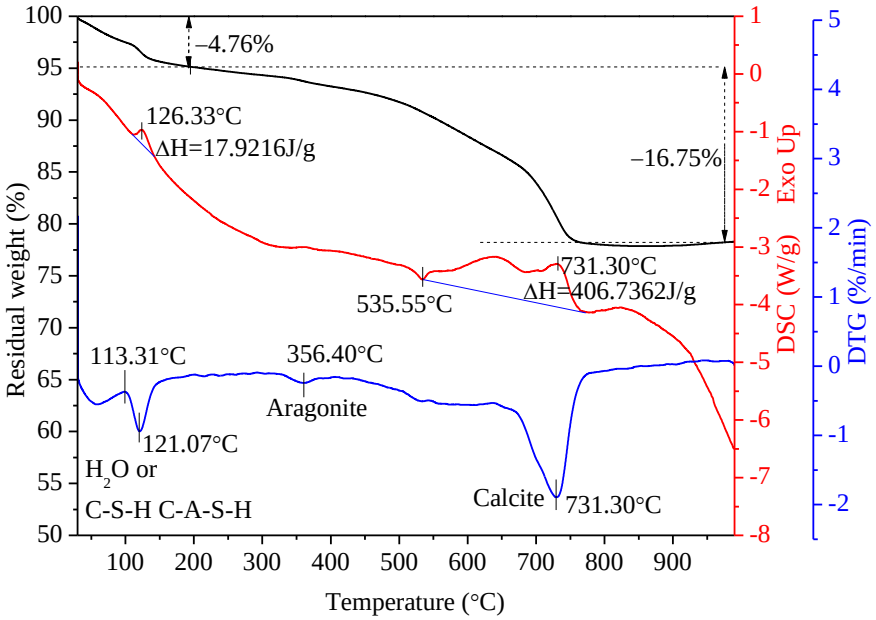


Figure 9. The TG, DTG, and DSC curves of the backfill paste (P1) cured for 90 days.

3.7. Discussion

The development of innovative backfill materials has many aims, the most important of which are to realize the use of a variety of different types of industrial solid wastes, to manage the fresh and hardened qualities such as fluidity, setting time, UCS, and stability, and to accomplish a one-part mixing method and a one-step mixing technique by adding water directly. According to the findings of the research, a geopolymer paste that is produced from a variety of solid wastes (accounting for 40–60% and containing inexpensive additives) results in excellent self-hardening for goaf backfill. The new backfill paste has the same fluidity, 28-d UCS, setting time, etc. as the OPC paste, but it is more stable under extreme circumstances.

The new perceptions of this study are as follows. (1) First, previous studies on grouting backfill materials have mostly used three or fewer solid wastes, while this paper uses four or more than four kinds of solid wastes, which is rare in previous studies. The preparation process, reaction process, and cementation mechanism involved in the application of multiple solid wastes have much to be explored. (2) In addition, the study of multiple solid waste backfill materials provides a research basis for the interchangeable use of similar components of solid waste and provides a wider utilization scheme for the resource utilization of industrial solid waste. (3) Finally, a new attempt to synthesize silica-alumina polymeric materials without the addition of strong alkali was achieved by revealing the reaction mechanism of inorganic silica-alumina-calcium-sodium composites.

Several alkali-activated mixture systems, as shown in prior studies, display excellent solidification under the necessary curing conditions, such as the systems of the FA-SR-Na_2SiO_3 solution [9], the FA-SR-Na_2SiO_3 solution incorporating hemihydrate gypsum [36], and the FA-CSG-NaOH solution [7], as well as, particularly, the systems of GBFS based materials [78,79], SR-CSG-GBFS based materials [10], FA-GBFS based materials [54], RM-FA based materials [6], CSG-GBFS based materials [2], and LP-GBFS based materials [12], etc. An alkaline activation system with excellent solidification consists primarily of silica-alumina precursors, alkaline activators, and calcium sources. In the blew reaction mechanism, all alkali-activated synthesis activities occur. The reaction process was examined utilizing the primary found elemental components Na, K, Ca, O, and Al to identify the final product, even though a Ca source is not required for the alkaline activation system. When amorphous silica-alumina precursors have been eroded and dissolved by alkaline activators, the resulting network structure is composed of Si and Al tetrahedrons that have

undergone reorganization and polycondensation [6]. The *M* cations, which include Na^+, K^+, and Ca^{2+}, balance out the negative charge provided by the Al tetrahedron, making the overall structure neutral and stable [65,80]. To counteract Coulomibic electrostatic repulsion, *M* combines with -OSi(OH), $Al(OH)^{4-}$, and other intermediate products. In addition, the empirical formula of geopolymeric product is $M_x[-(SiO_2)_y\text{-}AlO_2\text{-}]_x$, where Si/Al ratio *y* represents 1, 2, and 3, *M* denotes alkali metal cations such as Na^+, K^+, and Ca^{2+}, etc., and *x* represents the geopolymeric degree of Si and Al chain [6]. The final gel products that result from geopolymerization are either composed of N-A-S-H or (N,C)-A-S-H when the elemental components of the products meet the ratios 2Ca/Al < 1.0 and Si/Al > 1.0 [9,65]. When the ratios 2Ca/Al > 1.0 and Si/Al > 1.0 are satisfied in the elemental components of products, geopolymerization and hydration procedures result in the production of a combination of N-A-S-H and calcium (alumino)silicate hydrated C-(A)-S-H gels. This is because of the presence of excessive Ca^{2+} as a structure-changing cation [24]. Geopolymerization requires a certain quantity of Ca^{2+}, whereas excess Ca^{2+} combines with Si and Al monomers to create C-(A)-S-H gels. Consequently, it is possible to identify the final binder products by a mix of experimental procedures and quantitative calculations based on the geopolymerization and hydration reaction processes.

Following the basic synthesis components and synthesis procedures described above, it is simple to substitute raw materials in the creation of backfill paste. As silica-alumina precursors, the partial FA is replaced by GBFS and RM, and as a calcium source, the partial SRs are replaced by CSG and BRS. The LP and GP were employed to enhance the characteristics of the backfill paste. Some main alkaline activators, on the other hand, such as NaOH and Na_2SiO_3, are not advised owing to the strong erosion for the mixing and stirring container and the alkaline OH^- cation emission into the around environment. As shown in Figure 10, product mixtures of C-S-H, C-A-S-H, and (N,C)-A-S-H gels, together with many insoluble particles, are revealed, as is the cementation technique of fresh backfill paste using these wastes. Chemically, the dissolution of soluble inorganic salts produces reactive cations and ions, such as Ca^{2+}, Na^+, $[SiO_4]^{4-}$, $[AlO_4]^{5-}$, and OH^-, which result in binding owing to the formation of silicate gels or aluminosilicate gels. The fine aggregates in the backfill paste are made up of certain insoluble inorganic salts like $CaCO_3$, as well as some insoluble solids like mullite and quartz. According to the explanation provided by the cementation process, the chemical bonding of backfill paste requires soluble cations and ions as a prerequisite. Future research should examine how different types of salts, both inorganic (such as calcite carbonate, mullite, and quartz) and organic (such as calcium oxalate and carbohydrates), affect the properties of geopolymer backfill paste. This encourages the use of geopolymer backfill paste made from waste slags and organic-rich wastewater.

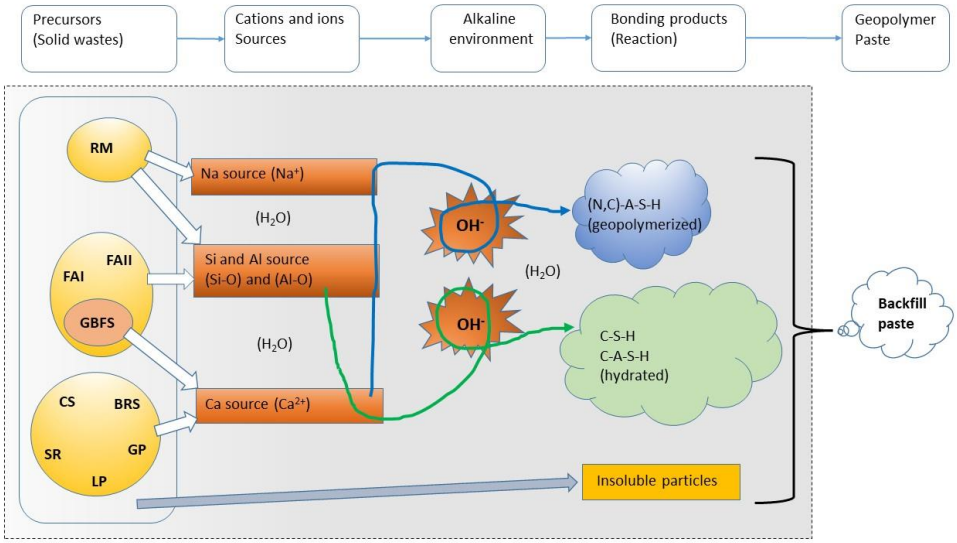


Figure 10. Reaction mechanism program of the new backfill paste P1 using diverse solid wastes.

The multi-solid waste cementitious material of this study was used as a grouting material for backfill and several recommendations still exist for practical engineering: (1) Raw materials are obtained close to the site, as transport costs increase application costs. (2) Pre-treatment of the raw material, because the required particle size range is key to improving workability.

4. Conclusions

The objective of this study was to evaluate the viability of employing various industrial solid wastes (SR, CSG, GBFS, FFAI, FFAII, RM, and BRS) to manufacture backfill paste for goaf grouting and to describe the fresh and hardened characteristics as well as the stability. The appropriate backfill paste mixing proportions in terms of the influences of raw materials were studied, and the resistances to shrinkage, permeability, and chemical attack were compared to OPC paste. In addition, the microstructure and cementation processes were uncovered for a comprehensive understanding of the physical and chemical bonding mechanisms underlying the nature of various solid wastes. The primary contributions based on the findings of the experiment are listed below.

(1) Direct synthesis of geopolymer paste for goaf backfill from a variety of solid wastes (FFAI, FFAII, SR, CSG, GBFS, RM, and BRS) and additives (LP, and GP) is possible with the addition of an adequate amount of water. The paste used as backfill hardens well and has no environmental impact on surrounding soils and water due to the seepage of less alkalinity. Even though the fresh and hardened characteristics of the new backfill paste are affected by the amounts of FFAI, RM, GBFS, and LP used, the paste can be adjusted to meet the requirements of goaf backfill because of its physical and chemical characteristics.

(2) With a W/B of 0.70, the optimal mass mixing ratio of new backfill paste P1 with different solid wastes is 1:4:1:2:1:1:1:1:2 (FFAI:FFAII:RM:CSG:SR:GBFS:BRS:GP:LP). Solid wastes (SR, CSG, GBFS, FFAI, FFAII, RM, and BRS) account for 46.0% by mass. Paste P1 has a 28-day UCS of 2.1 MPa and fluidity of 201 mm. The initial setting time was 920 min and the final setting time was 1220 min. In addition, after 90 days in terms of drying shrinkage, permeability, and Na_2SO_4 and NaCl solution attack, paste P1 was superior to the OPC paste.

(3) In alkaline circumstances, FFAI, FFAII, GBFS, and RM provide SiO_2 and Al_2O_3 precursors, while CSG, SR, GBFS, BRS, LP, and GP supply calcium sources such as CaO, $Ca(OH)_2$, and $CaCl_2$, among others. Furthermore, LP, RM, and GBFS raise the pH. The presence of (N,C)-A-S-H, C-S-H, and C-A-S-H gels from geopolymerization and hydration reactions in paste P1 is confirmed to play a crucial role in chemical cementation to support mechanical strength at a high pH of 12.37, while other unreacted particles ($CaCO_3$ and unreactive FA particles, etc.) act as the physical filling aggregate.

To conclude, a novel geopolymer paste for goaf backfill was developed employing a variety of industrial solid wastes such as SR, CSG, GBFS, FFAI, FFAII, RM, and BRS. The findings not only reveal the synthesis procedure but also offer stability data on fresh and hardened backfill paste. This study of diverse solid waste backfill materials provides a research basis for the interchangeable use of similar components of solid waste and provides a wider utilization scheme for the resource utilization of industrial solid waste. In addition, a new attempt to synthesize silica-alumina polymeric materials without the addition of strong alkali was achieved by revealing the reaction mechanism of inorganic silica-alumina-calcium-sodium composites. The combined application of diverse solid wastes may result in greater transportation costs due to long-distance transportation. In the following research effort, it is desirable to examine the mineral composition and reaction mechanism of the multi-solid waste-based cementitious materials, further clarifying the hardened nature by chemical techniques.

Author Contributions: Conceptualization, H.W. and X.Z.; formal analysis, H.G. and J.Y.; funding acquisition, H.W.; investigation, X.Z., H.G. and L.L.; methodology, H.W., X.Z., L.L. and J.Y.; project administration, H.W. and X.Z.; resources, X.Z.; software, H.G.; supervision, X.Z. and H.G.; validation, X.Z. and J.Y.; writing—original draft, H.W. and X.Z.; writing—review and editing, X.Z. and L.L. All authors have read and agreed to the published version of the manuscript.

Funding: This research was funded by the Tianjin Research Innovation Project for Postgraduate Students [grant number 201KJ078].

Institutional Review Board Statement: Not applicable.

Informed Consent Statement: Not applicable.

Data Availability Statement: Not applicable.

Conflicts of Interest: The authors declare that they have no known competing financial interest or personal relationships that could have appeared to influence the work reported in the paper.

References

1. Zhang, C.-Y.; Han, R.; Yu, B.; Wei, Y.-M. Accounting process-related CO_2 emissions from global cement production under Shared Socioeconomic Pathways. *J. Clean. Prod.* **2018**, *184*, 451–465. [CrossRef]
2. Li, W.; Yi, Y. Use of carbide slag from acetylene industry for activation of ground granulated blast-furnace slag. *Constr. Build. Mater.* **2020**, *238*, 117713. [CrossRef]
3. Andrew, R.M. Global CO_2 emissions from cement production, 1928–2018. *Earth Syst. Sci. Data* **2019**, *10*, 2213–2239. [CrossRef]
4. Cai, B.; Wang, J.; He, J.; Geng, Y. Evaluating CO_2 emission performance in China's cement industry: An enterprise perspective. *Appl. Energy* **2016**, *166*, 191–200. [CrossRef]
5. Guo, S.; Ma, C.; Long, G.; Xie, Y. Cleaner one-part geopolymer prepared by introducing fly ash sinking spherical beads: Properties and geopolymerization mechanism. *J. Clean. Prod.* **2019**, *219*, 686–697. [CrossRef]
6. Zhang, M.; Zhao, M.; Zhang, G.; Mann, D.; Lumsden, K.; Tao, M. Durability of red mud-fly ash based geopolymer and leaching behavior of heavy metals in sulfuric acid solutions and deionized water. *Constr. Build. Mater.* **2016**, *124*, 373–382. [CrossRef]
7. Qi, J.M.; Zhou, P.X.; Yang, D.; Wang, Z.X.; Li, B. Desulphurization mechanism and engineering practice of carbide slag. *Environ. Sci. Pollut. R.* **2022**, *29*, (59), 88519–88530. [CrossRef]
8. Zhao, X.; Wang, H.; Zhou, B.; Gao, H.; Lin, Y. Resistance of Soda Residue-Fly Ash Based Geopolymer Mortar to Acid and Sulfate Environments. *Materials* **2021**, *14*, 785. [CrossRef]
9. Zhao, X.; Liu, C.; Zuo, L.; Wang, L.; Zhu, Q.; Liu, Y.; Zhou, B. Synthesis and characterization of fly ash geopolymer paste for goaf backfill: Reuse of soda residue. *J. Clean. Prod.* **2020**, *260*, 121045. [CrossRef]
10. Guo, W.; Wang, S.; Xu, Z.; Zhang, Z.; Zhang, C.; Bai, Y.; Zhao, Q. Mechanical performance and microstructure improvement of soda residue–carbide slag–ground granulated blast furnace slag binder by optimizing its preparation process and curing method. *Constr. Build. Mater.* **2021**, *302*, 124403. [CrossRef]
11. Ma, C.; Zhao, B.; Guo, S.; Long, G.; Xie, Y. Properties and characterization of green one-part geopolymer activated by composite activators. *J. Clean. Prod.* **2019**, *220*, 188–199. [CrossRef]
12. Kim, M.S.; Jun, Y.; Lee, C.; Oh, J.E. Use of CaO as an activator for producing a price-competitive non-cement structural binder using ground granulated blast furnace slag. *Cem. Concr. Res.* **2013**, *54*, 208–214. [CrossRef]
13. Zhao, X.; Liu, C.; Wang, L.; Zuo, L.; Zhu, Q.; Ma, W. Physical and mechanical properties and micro characteristics of fly ash-based geopolymers incorporating soda residue. *Cem. Concr. Compos.* **2019**, *98*, 125–136. [CrossRef]
14. Thumrongvut, J.; Seangatith, S.; Phetchuay, C.; Suksiripattanapong, C. Comparative Experimental Study of Sustainable Reinforced Portland Cement Concrete and Geopolymer Concrete Beams Using Rice Husk Ash. *Sustainability* **2022**, *14*, 9856. [CrossRef]
15. Suksiripattanapong, C.; Krosoongnern, K.; Thumrongvut, J.; Sukontasukkul, P.; Horpibulsuk, S.; Chindaprasirt, P. Properties of cellular lightweight high calcium bottom ash-portland cement geopolymer mortar. *Case Stud. Constr. Mater.* **2020**, *12*, e00337. [CrossRef]
16. Phoo-ngernkham, T. Shear Bond Strength of Fa-Pc Geopoylmer under Different Sand to Binder Ratios and Sodium Hydroxide Concentrations. *Int. J. GEOMATE* **2018**, *14*, 52–57. [CrossRef]
17. Assi, L.; Carter, K.; Deaver, E.; Anay, R.; Ziehl, P. Sustainable concrete: Building a greener future. *J. Clean. Prod.* **2018**, *198*, 1641–1651. [CrossRef]
18. Hu, W.; Nie, Q.; Huang, B.; Shu, X.; He, Q. Mechanical and microstructural characterization of geopolymers derived from red mud and fly ashes. *J. Clean. Prod.* **2018**, *186*, 799–806. [CrossRef]
19. Zhao, J.; Wang, A.G.; Lyu, B.C.; Liu, K.W.; Chu, Y.J.; Ma, R.; Xu, H.Y.; Jing, Y.; Sun, D.S. Proportioning Factors of Alkali-Activated Materials and Interaction Relationship Revealed by Response Surface Modeling. *Materials* **2023**, *16*, 2042. [CrossRef]
20. McLellan, B.C.; Williams, R.P.; Lay, J.; van Riessen, A.; Corder, G.D. Costs and carbon emissions for geopolymer pastes in comparison to ordinary portland cement. *J. Clean. Prod.* **2011**, *19*, 1080–1090. [CrossRef]

21. Singh, N.; Middendorf, B. Geopolymers as an alternative to Portland cement: An overview. *Constr. Build. Mater.* **2020**, *237*, 117455. [CrossRef]
22. Guo, W.C.; Zhao, Q.X.; Sun, Y.J.; Xue, C.H.; Bai, Y.Y.; Shi, Y.X. Effects of various curing methods on the compressive strength and microstructure of blast furnace slag-fly ash-based cementitious material activated by alkaline solid wastes. *Constr. Build. Mater.* **2022**, *357*, 129397. [CrossRef]
23. Ibrahim, M.; Rahman, M.K.; Najamuddin, S.K.; Alhelal, Z.S.; Acero, C.E. A review on utilization of industrial by-products in the production of controlled low strength materials and factors influencing the properties. *Constr. Build. Mater.* **2022**, *325*, 126704. [CrossRef]
24. Wang, H.; Zhao, X.; Wang, T.; Su, L.; Zhou, B.; Lin, Y.; Mohan, S. Determination of Gel Products in Alkali-Activated Fly Ash-Based Composites Incorporating Inorganic Calcium Additives. *Adv. Mater. Sci. Eng.* **2022**, *2022*, 7476671. [CrossRef]
25. Oderji, S.Y.; Chen, B.; Ahmad, M.R.; Shah, S.F.A. Fresh and hardened properties of one-part fly ash-based geopolymer binders cured at room temperature: Effect of slag and alkali activators. *J. Clean. Prod.* **2019**, *225*, 1–10. [CrossRef]
26. Ye, N.; Yang, J.; Liang, S.; Hu, Y.; Hu, J.; Xiao, B.; Huang, Q. Synthesis and strength optimization of one-part geopolymer based on red mud. *Constr. Build. Mater.* **2016**, *111*, 317–325. [CrossRef]
27. National Development and Reform Commission of China. Implementing Scheme of Mainly Solid Waste Utilization; Beijing, China. 2011. Available online: https://www.docin.com/p-1851492371.html (accessed on 20 December 2022).
28. Shang, J.; Dai, J.-G.; Zhao, T.-J.; Guo, S.-Y.; Zhang, P.; Mu, B. Alternation of traditional cement mortars using fly ash-based geopolymer mortars modified by slag. *J. Clean. Prod.* **2018**, *203*, 746–756. [CrossRef]
29. Kumar, A.; Kumar, S. Development of paving blocks from synergistic use of red mud and fly ash using geopolymerization. *Constr. Build. Mater.* **2013**, *38*, 865–871. [CrossRef]
30. Pan, Z.; Tao, Z.; Cao, Y.; Wuhrer, R.; Murphy, T. Compressive strength and microstructure of alkali-activated fly ash/slag binders at high temperature. *Cem. Concr. Compos.* **2018**, *86*, 9–18. [CrossRef]
31. Haruna, S.; Fall, M. Time- and temperature-dependent rheological properties of cemented paste backfill that contains superplasticizer. *Powder Technol.* **2020**, *360*, 731–740. [CrossRef]
32. Saha, S.; Rajasekaran, C. Enhancement of the properties of fly ash based geopolymer paste by incorporating ground granulated blast furnace slag. *Constr. Build. Mater.* **2017**, *146*, 615–620. [CrossRef]
33. Lee, N.K.; Lee, H.K. Setting and mechanical properties of alkali-activated fly ash/slag concrete manufactured at room temperature. *Constr. Build. Mater.* **2013**, *47*, 1201–1209. [CrossRef]
34. Perná, I.; Hanzlíček, T. The setting time of a clay-slag geopolymer matrix: The influence of blast-furnace-slag addition and the mixing method. *J. Clean. Prod.* **2016**, *112*, 1150–1155. [CrossRef]
35. Nie, Q.; Hu, W.; Huang, B.; Shu, X.; He, Q. Synergistic utilization of red mud for flue-gas desulfurization and fly ash-based geopolymer preparation. *J. Hazard. Mater.* **2019**, *369*, 503–511. [CrossRef]
36. Wang, H.; Zhao, X.; Zhou, B.; Lin, Y.; Gao, H. Performance Optimization and Characterization of Soda Residue-Fly Ash Geopolymer Paste for Goaf Backfill: Beta-Hemihydrate Gypsum Alternative to Sodium Silicate. *Materials* **2020**, *13*, 5604. [CrossRef]
37. Zhao, X.; Liu, C.; Zuo, L.; Zhu, Q.; Ma, W.; Liu, Y. Preparation and characterization of press-formed fly ash cement incorporating soda residue. *Mater. Lett.* **2020**, *259*, 126852. [CrossRef]
38. He, K.; Shen, Z.; Zhang, B.; Sun, J.; Zou, H.; Zhou, M.; Zhang, Z.; Xu, H.; Ho, S.S.H.; Cao, J. Emission profiles of volatile organic compounds from various geological maturity coal and its clean coal briquetting in China. *Atmos. Res.* **2022**, *274*, 106200. [CrossRef]
39. Silva, D.; Filleti, R.; Musule, R.; Matheus, T.; Freire, F. A systematic review and life cycle assessment of biomass pellets and briquettes production in Latin America. *Renew. Sustain. Energy Rev.* **2022**, *157*, 112042. [CrossRef]
40. Hanjitsuwan, S.; Injorhor, B.; Phoo-Ngernkham, T.; Damrongwiriyanupap, N.; Li, L.-Y.; Sukontasukkul, P.; Chindaprasirt, P. Drying shrinkage, strength and microstructure of alkali-activated high-calcium fly ash using FGD-gypsum and dolomite as expansive additive. *Cem. Concr. Compos.* **2020**, *114*, 103760. [CrossRef]
41. Zhao, X.; Liu, C.; Zuo, L.; Wang, L.; Zhu, Q.; Wang, M. Investigation into the effect of calcium on the existence form of geopolymerized gel product of fly ash based geopolymers. *Cem. Concr. Compos.* **2019**, *103*, 279–292. [CrossRef]
42. Hanjitsuwan, S.; Phoo-Ngernkham, T.; Li, L.-Y.; Damrongwiriyanupap, N.; Chindaprasirt, P. Strength development and durability of alkali-activated fly ash mortar with calcium carbide residue as additive. *Constr. Build. Mater.* **2018**, *162*, 714–723. [CrossRef]
43. Niroshan, N.; Sivakugan, N.; Veenstra, R.L. Laboratory Study on Strength Development in Cemented Paste Backfills. *J. Mater. Civil Eng.* **2017**, *29*, 4017027. [CrossRef]
44. Li, H.; Wu, A.; Wang, H. Evaluation of short-term strength development of cemented backfill with varying sulphide contents and the use of additives. *J. Environ. Manag.* **2019**, *239*, 279–286. [CrossRef] [PubMed]
45. *JC/T 603-2004*; Standard Test Method for Drying Shrinkage of Mortar. 2004. Available online: http://www.cssn.net.cn/app/home/productDetail/a8105c02d10d9a7a92a9fef608f6879d (accessed on 14 February 2023). (In Chinese)
46. Sun, W.; Wang, H.J.; Hou, K.P. Control of waste rock-tailings paste backfill for active mining subsidence areas. *J. Clean. Prod.* **2018**, *171*, 567–579. [CrossRef]
47. Chi, M. Effects of dosage of alkali-activated solution and curing conditions on the properties and durability of alkali-activated slag concrete. *Constr. Build. Mater.* **2012**, *35*, 240–245. [CrossRef]

48. Wongsa, A.; Boonserm, K.; Waisurasingha, C.; Sata, V.; Chindaprasirt, P. Use of municipal solid waste incinerator (MSWI) bottom ash in high calcium fly ash geopolymer matrix. *J. Clean. Prod.* **2017**, *148*, 49–59. [CrossRef]
49. Sun, Q.; Tian, S.; Sun, Q.; Li, B.; Cai, C.; Xia, Y.; Wei, X.; Mu, Q. Preparation and microstructure of fly ash geopolymer. *J. Clean. Prod.* **2019**, *225*, 376–390. [CrossRef]
50. Kirkelund, G.M.; Magro, C.; Guedes, P.; Jensen, P.E.; Ribeiro, A.B.; Ottosen, L.M. Electrodialytic removal of heavy metals and chloride from municipal solid waste incineration fly ash and air pollution control residue in suspension—Test of a new two compartment experimental cell. *Electrochim. Acta* **2015**, *181*, 73–81. [CrossRef]
51. Elyamany, H.E.; Elmoaty, A.E.M.A.; Elshaboury, A.M. Setting time and 7-day strength of geopolymer mortar with various binders. *Constr. Build. Mater.* **2018**, *187*, 974–983. [CrossRef]
52. Nie, Q.; Hu, W.; Ai, T.; Huang, B.; Shu, X.; He, Q. Strength properties of geopolymers derived from original and desulfurized red mud cured at ambient temperature. *Constr. Build. Mater.* **2016**, *125*, 905–911. [CrossRef]
53. Lee, N.; Jang, J.; Lee, H. Shrinkage characteristics of alkali-activated fly ash/slag paste and mortar at early ages. *Cem. Concr. Compos.* **2014**, *53*, 239–248. [CrossRef]
54. Shi, C.; Day, R.L. Early strength development and hydration of alkali-activated blast furnace slag/fly ash blends. *Adv. Cem. Res.* **1999**, *11*, 189–196. [CrossRef]
55. Deb, P.S.; Nath, P.; Sarker, P.K. Drying Shrinkage of Slag Blended Fly Ash Geopolymer Concrete Cured at Room Temperature. *Procedia Eng.* **2015**, *125*, 594–600. [CrossRef]
56. Sadeghian, G.; Behfarnia, K.; Teymouri, M. Drying shrinkage of one-part alkali-activated slag concrete. *J. Build. Eng.* **2022**, *51*, 104263. [CrossRef]
57. Bakharev, T. Durability of geopolymer materials in sodium and magnesium sulfate solutions. *Cem. Concr. Res.* **2005**, *35*, 1233–1246. [CrossRef]
58. Chithiraputhiran, S.; Neithalath, N. Isothermal reaction kinetics and temperature dependence of alkali activation of slag, fly ash and their blends. *Constr. Build. Mater.* **2013**, *45*, 233–242. [CrossRef]
59. Bakharev, T.; Sanjayan, J.; Cheng, Y.-B. Sulfate attack on alkali-activated slag concrete. *Cem. Concr. Res.* **2002**, *32*, 211–216. [CrossRef]
60. Aiken, T.A.; Kwasny, J.; Sha, W.; Tong, K.T. Mechanical and durability properties of alkali-activated fly ash concrete with increasing slag content. *Constr. Build. Mater.* **2021**, *301*, 124330. [CrossRef]
61. Wang, W.-C.; Wang, H.-Y.; Lo, M.-H. The fresh and engineering properties of alkali activated slag as a function of fly ash replacement and alkali concentration. *Constr. Build. Mater.* **2015**, *84*, 224–229. [CrossRef]
62. Zhao, Z.; Guo, K.; Wang, X. A binder prepared by low-reactivity blast furnace slags for cemented paste backfill: Influence of super-fine fly ash and chemical additives. *Constr. Build. Mater.* **2022**, *327*, 126988. [CrossRef]
63. Provis, J.L.; Palomo, A.; Shi, C. Advances in understanding alkali-activated materials. *Cem. Concr. Res.* **2015**, *78*, 110–125. [CrossRef]
64. Yip, C.K.; Lukey, G.C.; Provis, J.L.; van Deventer, J.S. Effect of calcium silicate sources on geopolymerisation. *Cem. Concr. Res.* **2008**, *38*, 554–564. [CrossRef]
65. Garcia-Lodeiro, I.; Palomo, A.; Fernández-Jiménez, A.; Macphee, D. Compatibility studies between N-A-S-H and C-A-S-H gels. Study in the ternary diagram Na_2O-CaO-Al_2O_3-SiO_2-H_2O. *Cem. Concr. Res.* **2011**, *41*, 923–931. [CrossRef]
66. Zhai, Q.; Kurumisawa, K. Effect of accelerators on $Ca(OH)_2$ activated ground granulated blast-furnace slag at low curing temperature. *Cem. Concr. Compo.* **2021**, *124*, 104272. [CrossRef]
67. Leong, H.Y.; Ong, D.E.L.; Sanjayan, J.G.; Nazari, A. The effect of different Na_2O and K_2O ratios of alkali activator on compressive strength of fly ash based-geopolymer. *Constr. Build. Mater.* **2016**, *106*, 500–511. [CrossRef]
68. Wang, H.; Zhao, X.; Wang, J.; He, L.; Zhang, A.; Gao, H.; Yang, J.; Liang, L. Properties and Cementation Mechanism of Geopolymer Backfill Paste Incorporating Diverse Industrial Solid Wastes. *Materials* **2023**, *16*, 480. [CrossRef] [PubMed]
69. Haha, M.B.; Lothenbach, B.; Le Saout, G.; Winnefeld, F. Influence of slag chemistry on the hydration of alkali-activated blast-furnace slag—Part II: Effect of Al_2O_3. *Cem. Concr. Res.* **2012**, *42*, 74–83. [CrossRef]
70. Haha, M.B.; LE Saout, G.; Winnefeld, F.; Lothenbach, B. Influence of activator type on hydration kinetics, hydrate assemblage and microstructural development of alkali activated blast-furnace slags. *Cem. Concr. Res.* **2011**, *41*, 301–310. [CrossRef]
71. Walkley, B.; San Nicolas, R.; Sani, M.-A.; Rees, G.J.; Hanna, J.V.; van Deventer, J.S.; Provis, J.L. Phase evolution of C-(N)-A-S-H/N-A-S-H gel blends investigated via alkali-activation of synthetic calcium aluminosilicate precursors. *Cem. Concr. Res.* **2016**, *89*, 120–135. [CrossRef]
72. Bakharev, T. Geopolymeric materials prepared using Class F fly ash and elevated temperature curing. *Cem. Concr. Res.* **2005**, *35*, 1224–1232. [CrossRef]
73. Wei, X.; Li, D.; Ming, F.; Yang, C.; Chen, L.; Liu, Y. Influence of low-temperature curing on the mechanical strength, hydration process, and microstructure of alkali-activated fly ash and ground granulated blast furnace slag mortar. *Constr. Build. Mater.* **2021**, *269*, 121811. [CrossRef]
74. Shah, S.F.A.; Chen, B.; Oderji, S.Y.; Haque, M.A.; Ahmad, M.R. Improvement of early strength of fly ash-slag based one-part alkali activated mortar. *Constr. Build. Mater.* **2020**, *246*, 118533. [CrossRef]
75. Lodeiro, I.G.; Macphee, D.; Palomo, A.; Fernández-Jiménez, A. Effect of alkalis on fresh C–S–H gels. FTIR analysis. *Cem. Concr. Res.* **2009**, *39*, 147–153. [CrossRef]

76. Yu, P.; Kirkpatrick, R.J.; Poe, B.; McMillan, P.F.; Cong, X. Structure of Calcium Silicate Hydrate (C-S-H): Near-, Mid-, and Far-Infrared Spectroscopy. *J. Am. Ceram. Soc.* **2010**, *82*, 742–748. [CrossRef]
77. Fall, M.; Célestin, J.C.; Pokharel, M.; Touré, M. A contribution to understanding the effects of curing temperature on the mechanical properties of mine cemented tailings backfill. *Eng. Geol.* **2010**, *114*, 397–413. [CrossRef]
78. Petlovanyi, M.; Mamaikin, O. Assessment of an expediency of binder material mechanical activation in cemented rockfill. *ARPN J. Eng. Appl. Sci.* **2019**, *14*, 3492–3503.
79. Petlovanyi, M.V.; Zubko, S.A.; Popovych, V.V.; Sai, K.S. Physicochemical mechanism of structure formation and strengthening in the backfill massif when filling underground cavities. *Vopr. Khimii I Khimicheskoi Tekhnologii* **2020**, *6*, 142–150.
80. Fernandez-Jimenez, A.; Palomo, A.; Criado, M. Microstructure development of alkali-activated fly ash cement: A descriptive model. *Cem. Concr. Res.* **2005**, *35*, 1204–1209. [CrossRef]

Disclaimer/Publisher's Note: The statements, opinions and data contained in all publications are solely those of the individual author(s) and contributor(s) and not of MDPI and/or the editor(s). MDPI and/or the editor(s) disclaim responsibility for any injury to people or property resulting from any ideas, methods, instructions or products referred to in the content.